Single-Cell Transcriptome Analyses Reveal the Cell Diversity and Developmental Features of Human Gastric and Metaplastic Mucosa

Ayumu Tsubosaka[1], Daisuke Komura[1], Hiroto Katoh[1], Miwako Kakiuchi[1], Takumi Onoyama[1,2], Asami Yamamoto[1], Hiroyuki Abe[3], Yasuyuki Seto[4], Tetsuo Ushiku[3], Shumpei Ishikawa[1,5,*]

[1]Department of Preventive Medicine, Graduate School of Medicine, The University of Tokyo, 7-3-1 Hongo, Bunkyo-ku, 1130033, Tokyo, Japan

[2]Division of Gastroenterology and Nephrology, Department of Multidisciplinary Internal Medicine, School of Medicine, Faculty of Medicine, Tottori University, 36-1, Nishicho, Yonago, 683-8504, Tottori, Japan

[3]Dpartment of Pathology, Graduate School of Medicine, The University of Tokyo, 7-3-1, Hongo, Bunkyo-ku, 1130033, Tokyo, Japan

[4]Department of Gastrointestinal Surgery, Graduate School of Medicine, The University of Tokyo, 7-3-1, Hongo, Bunkyo-kyu, 1130033, Tokyo, Japan

[5]Division of Pathology, National Cancer Center Exploratory Oncology Research & Clinical Trial Center, 6-5-1, Kashiwanoha, Kashiwa, 277-8577, Chiba, Japan

*Correspondence: ishum-prm@m.u-tokyo.ac.jp

Abstract

The stomach is an important digestive organ with a variety of biological functions. However, due to the complexity of its cellular and glandular composition, the precise cellular biology has yet to be elucidated. In this study, we conducted single-cell RNA sequence analysis of the human stomach and constructed a 137,610-cell dataset, the largest cell atlas reported to date. By integrating this single-cell analysis with spatial cellular distribution analysis, we were able to clarify novel aspects of the developmental and tissue homeostatic ecosystems in the human stomach. We identified *LEFTY1+* as a potential stem cell marker in both gastric and intestinal metaplastic glands. We also revealed skewed distribution patterns

for PDGFRA+BMP4+WNT5A+ fibroblasts that play pivotal roles in, or even precede, the phenotypic changes from gastric to metaplastic mucosa. Our extensive dataset will function as a fundamental resource in investigations of the stomach, including studies on development, aging, and carcinogenesis.

INTRODUCTION

The stomach is an essential digestive organ found in many organisms. Its roles include storing and digesting food, releasing food to the intestine, secreting various digestive enzymes, and releasing hormones, e.g., gastrin and somatostatin (Voutilainen et al., 2002). Additionally, mucosal immunity is prevalent in the stomach through exposure to organisms/molecules swallowed during daily life (Nie and Yuan, 2020). The stomach mucosa consists of epithelial glands with a variety of compositions and functions that are biologically and histologically classified into three subtypes. One of the signature glands of the stomach, the fundic gland, is found in the fundus/corpus and composed mainly of chief cells, parietal cells, endocrine cells, and mucous cells. Another stomach-specific gland, the pyloric gland (PG), is found in the pylorus and composed mainly of mucous cells and endocrine cells. The other gland found in the stomach, the intestinal metaplasia (IM) gland, mimics the colorectal epithelial crypt and is a metaplastic gland associated with atrophy and caused by chronic inflammation, such as that resulting from *Helicobacter pylori* infection (Wroblewski et al., 2010).

Each stomach gland has a dedicated stem cell source (Kim and Shivdasani, 2016); however, in contrast to other digestive organs, such as the esophagus and intestines, the high cell diversity and complexity of the stomach has led to difficulty in identifying stomach epithelial stem cells related to developmental biology. Thus, similarities and differences in the developmental properties of the three gastric gland subtypes remain to be investigated. Although several stomach epithelial or pan stem cell markers, such as LGR5, CD44 (Kim and Shivdasani, 2016; Ye et al., 2018), and AQP5 (Tan et al., 2020), have been proposed, a consensus on such markers has yet to be reached. The identification of stem cells is important if we are to understand the development of tissues and tumorigenesis. Notably,

IM of the gastric mucosa is a well-known pathological condition that results directly in gastric carcinoma (Wroblewski et al., 2010); therefore, it is important to clarify how metaplastic mucosa arise from otherwise healthy gastric mucosa. Gastric stem cells may be transformed into intestinal stem cells (Jang et al., 2015; Simmini et al., 2014); however, the precise developmental properties of gastric and metaplastic glands have yet to be determined. Moreover, the differences and/or similarities between intestinal metaplastic gastric mucosa and genuine colorectal mucosa have not been clarified. Cell–cell communication through signaling molecules, such as cytokines, chemokines, and growth factors, is fundamental to establishing appropriate local tissue homeostasis in the human body. IM of the stomach can be triggered by pathological cycles of chronic inflammation and tissue repair; thus, the roadmap to IM may be affected by cellular communication in the environment of regenerative gastric mucosa, including that involving epithelial cells and various stromal cells, such as fibroblasts.

With the rapid development of single-cell RNA sequencing (scRNA-seq) and its associated analytical methods (Hao et al., 2021; Stuart et al., 2019), it has become feasible to construct global cell atlases with single-cell resolution and employ these to perform detailed analyses, e.g., identifying potential stem cell populations, clarifying developmental trajectories, and determining cell–cell communications between given cell types. To date, even the largest single cell atlas of the whole human body (The Tabula Sapiens Consortium, 2022) has not included the stomach scRNA-seq dataset. Busslinger et al. (2021) reported a scRNA-seq profile of human upper gastrointestinal tract; however, a specific stomach scRNA-seq dataset has been lacking.

In the present study, we constructed the largest ever transcriptional cell atlas of adult human gastric tissues using scRNA-seq and used it for the analyses as follows: profiling the global cellular diversity of the complexed gastric mucosa in healthy and metaplastic tissues, identifying possible stem cell populations in gastric glands, and discovering novel cell–cell communications related to homeostasis in the studied conditions. By integrating sophisticated bioinformatics analysis of scRNA-seq data with high-resolution spatial distribution analyses of specific mRNA molecules in human tissues, we not only

identified a possible stem cell cluster common among the gastric glands but also clarified the spatially and functionally defined biological roles of BMP4-secreting fibroblasts found in either healthy or metaplastic gastric mucosa. As a resource that includes a scRNA-seq dataset with 137,610 cells, our human stomach cell atlas could help researchers provide new insights in the fields of gastric development, gastric stem cell biology, and gastric carcinogenesis.

RESULTS and DISCUSSION

Single-cell atlas of normal and IM gastric mucosa

We obtained gastric tissues from 15 patients who underwent gastrectomy at The University of Tokyo Hospital, and their scRNA-seq data were combined with those of 9 patients from Stanford University (Sathe et al., 2020) and 9 patients from Tsinghua University (Zhang et al., 2019). These nontumor gastric tissues were derived from a spectrum of healthy and disease states, including histologically normal gastric tissues, gastric cancers, intestinal metaplastic mucosa, and gastritis specimens (Table S1).

After exclusion of low quality and doublet cells, 137,610 cells were retained (see Methods; Figure 1A). After batch effect correction, unsupervised clustering analysis was used to identify 35 clusters. We merged the clusters into seven major cell lineages based on differential gene expression as follows (Figures 1B and 1C): 39,169 epithelial cells (characterized by *KRT19, TFF1,* and *PGA4*), 71,360 B and plasma cells (B cells: *MS4A1*; plasma cells: *IGHG1, IGHA1, IGKC,* and *IGHG4*), 15,778 T cells (*CD3D*), 2,002 myeloid cells (*FCGR3A* and *ITGAM*), 5,225 fibroblasts (*COL1A1* and *ACTA2*), 3,071 endothelial cells (*PECAM1* and *VWF*), and 1,005 mast cells (*TPSAB1*). The proportions of cell types in each clinical procedure or institution are shown in Figure 1D. Some of the samples in our institution contained exclusively higher proportions of B and plasma cells; thus, we excluded these samples from this research. Biopsy specimens from Tsinghua University had substantially larger proportions of epithelial cells, consistent with the fact that gastric biopsies mainly obtain surface mucosa. Additionally,

surgical specimens from Stanford University and our institution had a larger proportion of nonepithelial cells. Overall, by combining three large RNA-seq datasets of the stomach with different clinical procedures and disease states, we successfully obtained a well-balanced and diverse cell atlas of the human stomach.

Epithelial cells

Subcluster determination

We subclustered 39,169 epithelial cells into 11 clusters comprising foveolar subtypes (characterized by *MUC5AC, GKN1, GKN2, TFF1, TFF2,* and *ADH1C*), PG/neck cells (*MUC6, PGC,* and *TFF2*), chief cells (*PGA4, PGC,* and *LIPF*), parietal cells (*ATP4A, ATP4B,* and *CKB*), enterocytes (*FABP1, FABP2,* and *CDH17*), goblet cells (*MUC2, TFF3,* and *SPINK4*), neuroendocrine (NE) cells (*GAST, SST, GHRL, CHGA, MAOB,* and *CHGB*), and proliferating cells (*MKI67, HMGB2,* and *STMN1*) (Figures 1E–G; Figure S1A). The proportion of cells in each subcluster along with the severeness of IM is shown in Figures 1H and 1I, showing the increase in the number of enterocytes and goblet cells in the severe IM samples.

First, we focused on the characteristics of NE cells because they might represent the interpretable characteristics of each gastric and metaplastic gland. NE cells commonly expressed *CHGA* and *CHGB* and were clustered into at least five populations, including G cells and D cells, based on the expression of hormones or enzymes, such as *SST* (D cell marker), *GHRL* (X/A-like cell marker), *GAST* (G cell marker), and *MAOB* (enterochromaffin cell marker; Figures S1B and S1C; Busslinger et al. (2021)). Some NE cells expressed *LHB*, as reported by Busslinger et al. (2021). Interestingly, some NE cells expressed *REG4*, a specific marker of metaplastic mucosa (Zhang et al., 2019). Some *REG4*+ NE cells also expressed *GCG* and *PYY*, which are specific to enteroneuroendocrine cells (Gunawardene et al., 2011). Notably, the severeness of IM (Figure 1I) was correlated with the frequency of *REG4*+ NE cells (Figures S1B and S1C), suggesting that IM of the stomach consists of NE cells with the endocrine features of genuine colonic enteroneuroendocrine cells. The phenotypic similarity between IM of the

stomach and colonic mucosa indicates that the regeneration of atrophic gastric mucosa generates metaplastic mucosa that resembles, both histologically and functionally, genuine colorectal mucosa.

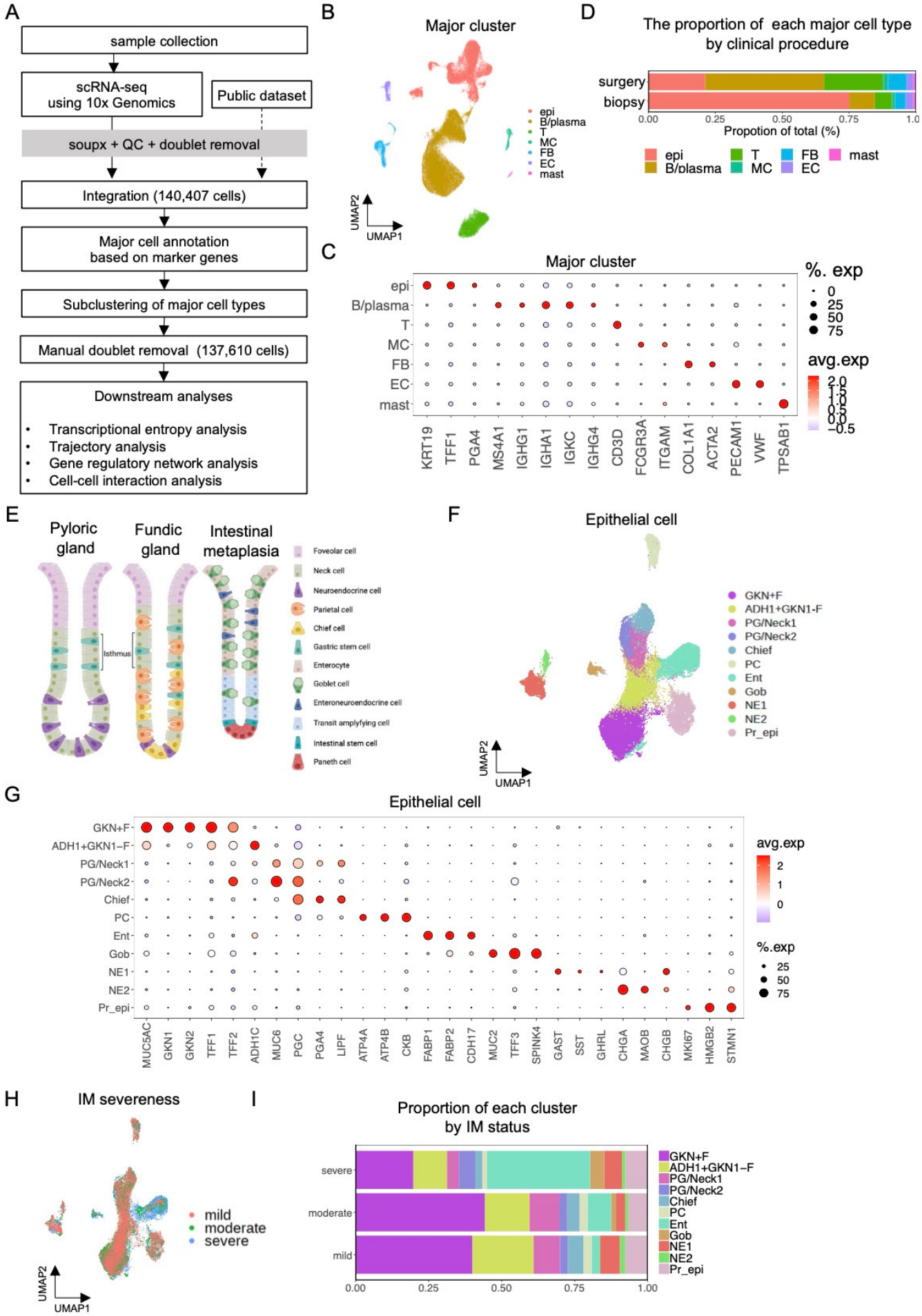
A
sample collection
scRNA-seq using 10x Genomics
Public dataset
soupx + QC + doublet removal
Integration (140,407 cells)
Major cell annotation based on marker genes
Subclustering of major cell types
Manual doublet removal (137,610 cells)
Downstream analyses
Transcriptional entropy analysis
Trajectory analysis
Gene regulatory network analysis
Cell-cell interaction analysis
B
Major cluster
epi
B/plasma
T
MC
FB
EC
mast
UMAP2
UMAP1
D
The proportion of each major cell type by clinical procedure
surgery
biopsy
Propotion of total (%)
C
Major cluster
%. exp
avg.exp
KRT19
TFF1
PGA4
MS4A1
IGHG1
IGHA1
IGKC
IGHG4
CD3D
FCGR3A
ITGAM
COL1A1
ACTA2
PECAM1
VWF
TPSAB1
E
Pyloric gland
Fundic gland
Intestinal metaplasia
Isthmus
Foveolar cell
Neck cell
Neuroendocrine cell
Parietal cell
Chief cell
Gastric stem cell
Enterocyte
Goblet cell
Enteroneuroendocrine cell
Transit amplyfying cell
Intestinal stem cell
Paneth cell
F
Epithelial cell
GKN+F
ADH1+GKN1-F
PG/Neck1
PG/Neck2
Chief
PC
Ent
Gob
NE1
NE2
Pr_epi
G
Epithelial cell
avg.exp
%.exp
MUC5AC
GKN1
GKN2
TFF1
TFF2
ADH1C
MUC6
PGC
PGA4
LIPF
ATP4A
ATP4B
CKB
FABP1
FABP2
CDH17
MUC2
TFF3
SPINK4
GAST
SST
GHRL
CHGA
MAOB
CHGB
MKI67
HMGB2
STMN1
H
IM severeness
mild
moderate
severe
I
Proportion of each cluster by IM status
severe
moderate
mild

129

Figure 1. Major cell and epithelial cell clustering in stomach mucosa.

(A) Overview of the comprehensive scRNA-seq analysis workflow.

(B) UMAP showing the 7 major cell types identified by scRNA-seq (137,610 cells) of all cells after QC.

(C) Representative major cell marker genes. Size and color of circles show the percentage of cells expressing genes and average gene expression, respectively.

(D) Proportion of major cell types according to clinical procedure. Biopsy specimens had larger proportions of epithelial cells and surgical specimens had a larger proportion of nonepithelial cells.

(E) Scheme of each epithelial cell-type in the pyloric gland, fundic gland, and metaplastic mucosa.

(F) UMAP showing subclusters of epithelial cells (39,169 cells) identified by scRNA-seq.

(G) Representative epithelial cell marker genes. Size and color of circles show the percentage of cells expressing genes and average gene expression, respectively.

(H) UMAP showing the IM state tissue from which each cell was derived. See methods for IM status determination.

(I) Proportion of epithelial cell types according to IM status. IM severe samples had a larger proportion of goblet and enterocytes.

Abbreviations: UMAP, Uniform Manifold Approximation and Projection; QC: quality check; epi: epithelial cells; MC: myeloid cells; FB: fibroblasts; EC: endothelial cells, F: foveolar cells, PG: pyloric gland cells, PC: parietal cells, Ent: enterocytes, Gob: goblet cells, NE: neuroendocrine cells, Pr_epi: proliferating epithelial cells.

150 Foveolar cells, surface mucous cells for which the biological characteristics are known to differ
151 between gastric and metaplastic mucosa (Kim and Shivdasani, 2016), were clustered into two distinct
152 populations: GKN1+F cells and ADH1+GKN1-F cells (Figures 1F and 1G; Figure S1A). Encoded by *GKN1*,
153 gastrokine-1 is a stomach-specific protein with various functions, including modulating cell cycle
154 progression, cellular proliferation, and antibiotic, anti-inflammation, and antiapoptotic actions
155 (Alarcón-Millán et al., 2019). Encoded by *ADH1C*, alcohol dehydrogenase 1C is often discussed in the
156 context of ethanol metabolism (Edenberg and McClintick, 2018); however, the relationships between its
157 expression and *H. pylori* infection and IM have been investigated previously, and it may be relevant to the
158 metabolism of retinol acid (Matsumoto et al., 2005). In human stomach specimens, GKN1 expression was
159 observed in gastric mucosa but not in metaplastic mucosa (Figures S1D and S1E); moreover, the spatial
160 distributions of the distinct GKN1+F and ADH1+GKN1-F populations showed clear gradation patterns in
161 the superficial and deeper layers, respectively, of the gastric mucosa (Figures S1D and S1E). Thus, a
162 combination of scRNA-seq analysis and spatial identification of specific populations confirmed the
163 histological distributions of the distinct foveolar subtypes, consistent with the findings of previous studies
164 (Mao et al., 2012; Westerlund et al., 2007); moreover, the results suggested that the ADH1+GKN1-F and
165 GKN+F populations represent immature (deeper layer) and mature (surface layer) foveolar epithelium,
166 respectively.

167 The transcription factor *NKX6-3* is known to be a distinctive positive modulator of *GKN1*
168 (Alarcón-Millán et al., 2019), and its expression is specific to the gastric mucosa (Choi et al., 2008). NE
169 cells showed characteristically higher expression of *NKX6-3*, especially G and D cells (Figures S1A and
170 S1C). We also found that non-NE cells in the stomach showed various degrees of positivity for *NKX6-3*
171 (Figure S1A), indicating that *NKX6-3* has a wider range of biological functions in various stomach cells
172 than was previously expected. Indeed, a previous study showed that *NKX6-3* inactivation in the stomach
173 led to overexpression of *CDX2* and reduced expression of *SOX2* (Yoon et al., 2015).

174 Gastric fundic glands and PGs are composed of foveolar epithelium, isthmus, and neck cells

175 (Figures 1E and 1F). Using our integrated scRNA-seq dataset, we identified diverse cell populations,
176 including those of the neck areas of gastric glands, which we termed PG/Neck cells (Figures 1E–G).
177 Intriguingly, we identified two distinct PG/neck cell populations: PG/Neck1 and PG/Neck2 cells (Figures
178 1F and 1G). Some PG/Neck2 cells expressed *MUC6* and/or *TFF2*; thus, they included pyloric as well as
179 fundic mucous gland cells (Wuputra et al., 2021; Zhang et al., 2019). Higher expression of *MUC6* and
180 *TFF2* is reportedly related to spasmolytic polypeptide-expressing metaplasia (Nam et al., 2010), which is
181 associated with chronic inflammation and IM of the stomach (Radyk et al., 2018). Consistent with this
182 notion, the PG/Neck2 population included cells that expressed *CLDN2* and *TFF3*, known markers for
183 intestinal and goblet cells, respectively (Escaffit et al., 2005; Zhang et al., 2019). Thus, the PG/Neck2
184 cells apparently include highly diverse cell populations covering the fundic/pyloric and metaplastic
185 glands. These cells also expressed *AQP5*, *ODAM*, and *PRR4* as differentially expressed markers, all of
186 which are known salivary gland markers (Hosoi, 2016; Huang et al., 2021), although the underlying
187 physiological basis of the similarity between the stomach and saliva is unclear. Notably, *AQP5* was
188 proposed as a gastric stem cell marker in a previous study (Tan et al., 2020).
189

190 **Transcriptional entropy and gene expression trajectory analyses of epithelial cells reveal the**
191 **LEFTY1+ cell population as a potential stem cell cluster common to the gastric and metaplastic**
192 **glands**

193 The distinct stem cell populations in the gastric and metaplastic mucosa are yet to be clarified; however,
194 it is hypothesized that the stem cell compartment exists in the PG/Neck cells among the cellular clusters
195 identified here (Han et al., 2019; Kim and Shivdasani, 2016). To determine the possible stem cells of the
196 stomach glands, we performed transcriptional entropy analysis, calculating the stemness score based on
197 the number of expressed genes per cell (see Methods; Gulati et al., 2020). The stemness score was
198 considered an indicator of the differentiation states of each cell: higher entropy suggests that the cell is in
199 a more immature state (Gulati et al., 2020). In our analysis, PG/Neck2 cells had significantly higher

stemness scores compared with those of PG/Neck1 cells ($p<2.2e-16$, Figure 2A); therefore, we hypothesized that the PG/Neck2 cluster contained possible stem cells. To explore the stem cell populations of the stomach epithelial cells as well as their developmental paths, we performed unsupervised trajectory analysis (Cao et al., 2019) in which the differentiation dynamics of gene expression were visualized (Figures 2B–E). This analysis revealed two separated lineages, namely the normal gastric lineage and the intestinal metaplastic lineage, which were characterized by *SOX2* and *CDX2* enrichment, respectively (Figures 2B and 2C), consistent with their known functions in the respective development of the stomach and intestine (Kim and Shivdasani, 2016). Interestingly, we found a tiny population in PG/Neck2 cells (we termed these “linking cells”) located between the gastric and intestinal routes (Figure 2D). In the PG/Neck2 population, these distinct cells were thought to be possible stem cells because expression of the stem-associated markers (e.g., *AQP5, LGR5, SMOC2, ASCL2, TNFRSF19, EPHB2, CD44,* and *PROM1*; Guo and Frenette, 2014; Jang et al., 2013, 2017; Kim and Shivdasani, 2016; Tan et al., 2020; Ye et al., 2018) was relatively high (Figures S2A and S2B). Moreover, pseudotime analysis showed chronological trajectories from the “linking cell” population to various paths of the stomach epithelia (Figure 2E). Among PG/Neck2 cells, the candidates of specific markers for “linking” cells were *LEFTY1*, *OLFM4*, and *CLDN4* in differentially expressed genes (Figure 2F). Whereas *OLFM4* and *CLDN4* were expressed not only in linking cells, but in the enterocytes and goblet cells (Figures S2A and S2B), *LEFTY1* was highly enriched in the “linking” cells (Figure 2G). LGR5, a representative stem cell marker, was also expressed in the “linking” cells (Figure 2G). Above all, *LEFTY1* was distinguished as a differentially expressed gene in the “linking” cells with possible stem cell properties.

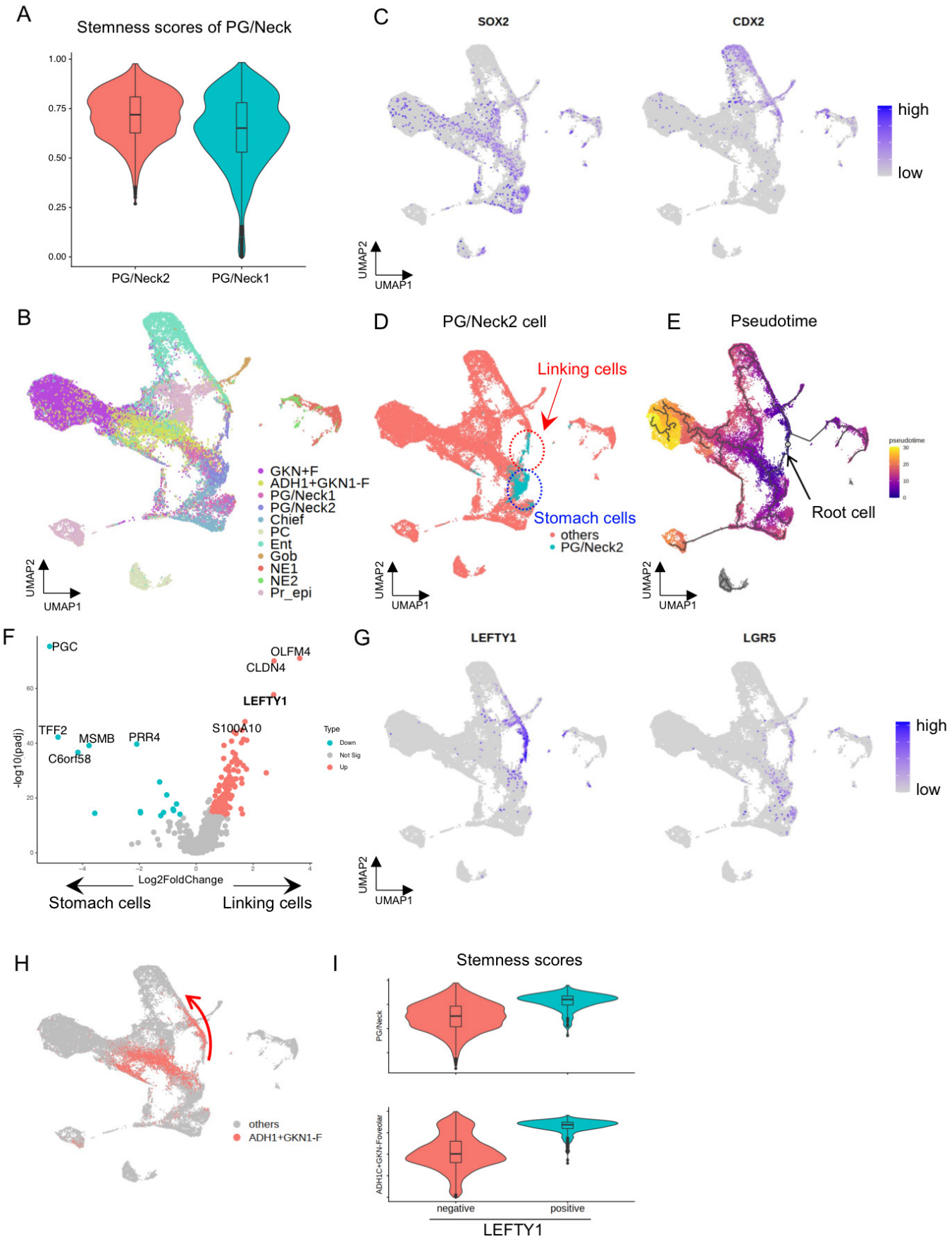
A
Stemness scores of PG/Neck
1.00
0.75
0.50
0.25
0.00
PG/Neck2
PG/Neck1
C
SOX2
CDX2
high
low
UMAP2
UMAP1
B
GKN+F
ADH1+GKN1-F
PG/Neck1
PG/Neck2
Chief
PC
Ent
Gob
NE1
NE2
Pr_epi
UMAP2
UMAP1
D
PG/Neck2 cell
Linking cells
Stomach cells
others
PG/Neck2
UMAP2
UMAP1
E
Pseudotime
pseudotime
Root cell
UMAP2
UMAP1
F
PGC
OLFM4
CLDN4
LEFTY1
S100A10
TFF2
MSMB
PRR4
C6orf58
Type
Down
Not Sig
Up
-log10(padj)
Log2FoldChange
Stomach cells
Linking cells
G
LEFTY1
LGR5
high
low
UMAP2
UMAP1
H
others
ADH1+GKN1-F
I
Stemness scores
PG/Neck
ADH1C+GKN-Foveolar
negative
positive
LEFTY1

221

222

Figure 2. Trajectory analysis of epithelial cells identified a possible novel stem cell marker, LEFTY1.

(A) The comparison of stemness scores between PG/Neck1 and 2. The score of PG/Neck2 is significantly higher than PG/Neck1 ($p<2.2e-16$, two-sided Welch's t test).

(B) UMAP showing each subcluster shown in Figure 1F. UMAP coordinates of epithelial cells was re-calculated by trajectory inference analysis. See Methods for details.

(C) *SOX2* and *CDX2* expression (master regulators of the stomach and intestine, respectively) in epithelial cells. *SOX2* was expressed in the normal gastric cells, whereas *CDX2* was in the intestinal metaplastic cells.

(D) UMAP showing two separate groups of PG/Neck2 cells: linking cells, which were located between the metaplastic and stomach cells, and those within the other stomach cells.

(E) Pseudotime trajectory analysis displayed on the UMAP plot. It is based on the assumed root cell (arrow), which was determined manually among LEFTY1+ positive cells.

(F) Volcano plot showing the top differentially expressed genes between the two PG/Neck2 groups shown in Figure 2D (linking cells and stomach cells). *OLFM4*, *CLDN4*, and *LEFTY1*, were top differentially expressed genes in the linking cells.

(G) *LEFTY1* and *LGR5* expression in epithelial cells. Both genes were expressed in the linking cells.

(H) ADH1+GKN1-F cells on the UMAP plot. Some ADH1+GKN1-F cells on the routes of metaplastic lineages (arrow) expressed *LEFTY1* as shown in Figure 2G.

(I) The comparison of stemness scores between LEFTY1+ and LEFTY1− cells in each PG/Neck2 cell cluster and ADH1+GKN-F cell cluster. The score of each LEFTY1+ population is significantly higher than LEFTY1- population ($p<2.2e-16$, two-sided Welch's t test).

Abbreviations: padj, adjusted p-value.

246 *LEFTY1*, the product of which is a secreted protein and transforming growth factor-beta (TGF-
247 β) superfamily member, has been extensively studied in the developmental stage and is known to play a
248 role in determining left–right asymmetry (Kosaki et al., 1999; Meno et al., 1998). LEFTY1 inhibits SMAD
249 signaling by binding to Cripto-1 and blocks Nodal in the development of mice (Tabibzadeh and
250 Hemmati-Brivanlou, 2006). Additionally, scRNA-seq analysis of Barrett's esophagus has shown that
251 *LEFTY1* is a potential marker of Barrett's esophagus precursors in human (Owen et al., 2018). Zabala et
252 al. (2020) showed that LEFTY1 and bone morphogenetic protein (BMP) 7 maintained long-term
253 proliferation and differentiation of human mammary gland cells, respectively, through a mechanism
254 whereby LEFTY1 binds to BMPR2 and prevents BMP7/BMPR2-mediated SMAD activation. In the
255 present study, some ADH1+GKN1-F cell routes specifically found in the metaplastic lineage also
256 expressed *LEFTY1* (Figures 2G and 2H). To determine whether *LEFTY1* is an actual marker of stem
257 cells and investigate their possible roles in the development of stomach mucosa, we divided both
258 PG/Neck2 and ADH1+GKN1- F cells into two clusters each, i.e., *LEFTY1*+ and *LEFTY1*−, respectively.
259 First, *LEFTY1*+ cells showed significantly higher stemness scores in both PG/Neck2 and ADH1+GKN1-
260 F cell populations ($p<2.2e-16$, Figure 2I). Pseudotime plotting showed that *LEFTY1* was highly
261 expressed in cells at the earliest time point and commonly in all types of stomach glands (Figures S2C–
262 H). Notably, some conventional stemness-associated genes, such as *CD44* and *EPHB2*, were also
263 expressed in similar time courses to those in which *LEFTY1* was expressed (Figures S2C–E). In the
264 middle of pseudotime, cell division marker, *MKI67*, were expressed around the "proliferative epithelial"
265 population (Figures S2C–E). Compared with other conventional stem cell markers or with stem cell- or
266 cancer stem cell-enriched markers (e.g., *AQP5, LGR5, SMOC2, ASCL2, TNFRSF19, EPHB2, CD44,*
267 and *PROM1*; Guo and Frenette, 2014; Jang et al., 2013, 2017; Kim and Shivdasani, 2016; Tan et al.,
268 2020; Ye et al., 2018), LEFTY1+ cells were more highly expressed and specifically existed in a "linking"
269 cell population (Figure 2G; Figures S2A and S2B). Cell cycle analysis showed that the ratio of G2/M
270 cells was lowest in *LEFTY1*+ PG/Neck cells (Figure S2I), which was compatible with their quiescence.

IHC showed that LEFTY1+ cells existed in gastric pyloric and fundic glands at very low frequencies and were spatially located mainly around the so-called isthmus regions (Figure 3A), consistent with the consideration of the histological isthmus region as a stem cell zone (Figure 1E; Han et al., 2019; Kim and Shivdasani, 2016). Contrastingly, in the intestinal metaplastic mucosa, LEFTY1+ cells were observed at much higher frequencies and were spatially located at the base of crypts (Figure 3A), consistent with the knowledge that intestinal stem cells reside at crypt bases (Spit et al., 2018). These spatial data support the hypothesis that *LEFTY1* is a novel marker of gastric stem cells. LEFTY1+ cell frequencies were highest in the metaplastic glands, followed by the PGs and fundic glands, respectively (Figure 3A). LEFTY1 staining showed two different patterns: a moderate cytoplasmic staining pattern and an intense dot signal pattern. However, the functional differences, if any, of LEFTY1 in relation to these staining patterns are not clear, as reported previously in an esophageal study (Owen et al., 2018).

We performed RNA *in situ* hybridization (RNA-ISH) of *LEFTY1* and *LGR5* (Figure 3A), finding that a portion of *LGR5*+ cells coexpressed *LEFTY1* in the pyloric and metaplastic mucosa. Additionally, scRNA-seq analysis and immunofluorescent staining showed that subsets of the CD44+ and/or EPHB2+ possible stem cells coexpressed LEFTY1 (Figures 3B–E). In our spatial analysis of human gastric tissues, the colocalization of LEFTY1 with other stem cell markers and the low frequency of LEFTY1+ cells among other stem-marker-positive cells strongly suggest that LEFTY1 is an actual candidate stem cell marker. LEFTY1+ cells can be considered common stem cells in both gastric and metaplastic glands based on our trajectory and pseudotime analyses; however, we found that EPHB2 was expressed in LEFTY1+ cells in the metaplastic mucosa but not in the normal gastric mucosa (Figure 3E). We hypothesize that, during IM, a phenotypic change occurs in LEFTY1+ stem cells in the normal gastric gland and they acquire the distinctive properties of intestinal stem cells by obtaining the EPHB2+ phenotype.

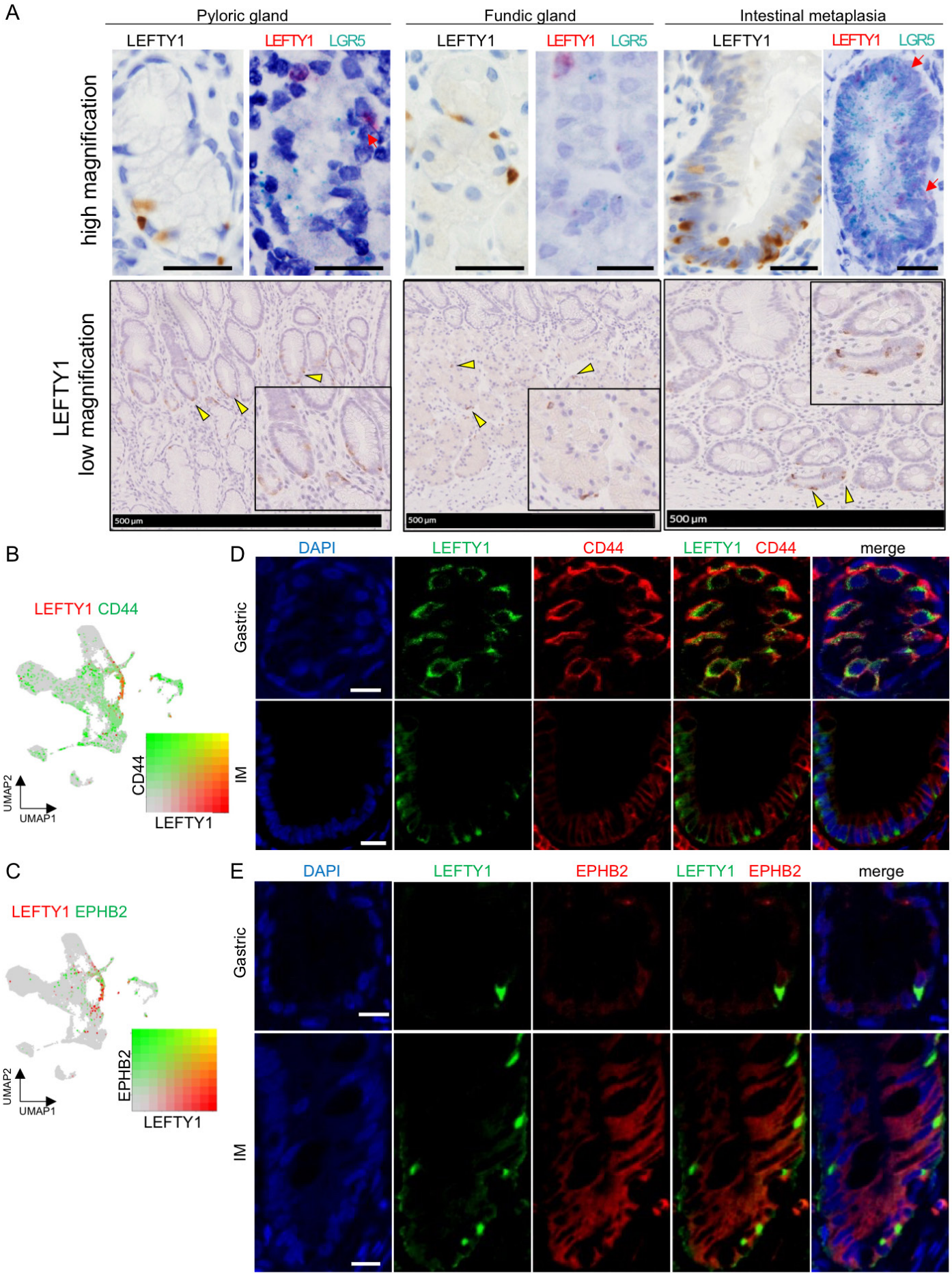
A
Pyloric gland
Fundic gland
Intestinal metaplasia
LEFTY1
LEFTY1 LGR5
high magnification
LEFTY1
low magnification
500 µm
B
LEFTY1 CD44
UMAP2
UMAP1
CD44
LEFTY1
C
LEFTY1 EPHB2
EPHB2
D
DAPI
LEFTY1
CD44
merge
Gastric
IM
E

296

297

298 **Figure 3. Coexpression of LEFTY1 and conventional gastrointestinal stem cell marker genes in**
299 **epithelial cells.**

300 (A) Top: IHC of LEFTY1 (lefthand boxes) and RNA-ISH [righthand boxes: LEFTY1 (red) and LGR5
301 (green)]. Staining and *in situ* hybridization were performed in pyloric glands, fundic glands, and
302 intestinal metaplasia (as shown). Some cells coexpressed LEFTY1 and LGR5 (arrows). Scale
303 bar: 25 μm. Bottom: LEFTY1 low magnification of IHC. LEFTY1 expression was observed in the
304 conventional stem cell zone. Arrowheads: LEFTY1+ cells.

305 (B, C) Combined feature plots showing CD44 and EPHB2 (green) expression with LEFTY1 (red).
306 Coexpressing cells are shown in yellow.

307 (D, E) Immunofluorescence of LEFTY1 (green) and CD44/EPHB2 (red) in the intestinal metaplasia
308 and gastric mucosa. (D) Area of clustered LEFTY1+ cells in gastric mucosa was selected for
309 clarity. Scale bar: 10 μm.

310

311 **Gene regulatory network analysis of stomach epithelial cells**

312 To investigate the global gene regulatory network in gastric epithelial cells, we analyzed the activity of
313 transcriptional programs in each epithelial cell-type by integrating the expression of transcription factors
314 and their downstream target genes (Aibar et al., 2017; Van de Sande et al., 2020). Through gene
315 regulatory network analysis, we obtained regulon activity scores in each cell-type (Figure 4A; Figure S3A).
316 Our results were consistent with those of previous studies; for example, NE cells showed high paired box
317 6 (PAX6) or achaete-scute family BHLH transcription factor 1 (ASCL1) activities, as reported previously
318 (Kim and Shivdasani, 2016), parietal cells showed high estrogen-related receptor gamma and beta activity,
319 which is known to regulate ATP4A and ATP4B (Zhang et al., 2019), and enterocytes showed high scores
320 for the colon-specific transcription factors CDX1 and CDX2 (Almeida et al., 2003) (Figure S3A). These
321 results demonstrate the utility of gene regulatory network analysis for correctly identifying transcription
322 factor activity.

323 Notably, high HOXB13 regulon activity was observed in LEFTY1+ clusters (in both LEFTY1+
324 PG/Neck and LEFTY1+ ADH+F clusters; Figure 4A). As expected, SOX2 and CDX2 regulon activities
325 were high in normal and metaplastic mucosa, respectively (Figure 4B), whereas HOXB13 regulon
326 activity was limited to the possible stem cell region and metaplastic epithelial cells (Figure 4B). Thus, the
327 HOXB13 regulon might play an important role in the LEFTY1+ cells found in the metaplastic mucosa.
328 *HOXB13*, the expression of which is almost exclusively found in the prostate and intestine, has been
329 extensively studied in prostate cancer because both somatic and germline variants of *HOXB13* are
330 associated with this cancer (Morgan and Pandha, 2017; Yu et al., 2020). HOXB13 is also known to
331 downregulate the expression of TCF4 and its target MYC in colon cancer cells (Xie et al., 2019).
332 Additionally, *HOXB13* expression is higher in left-sided colon cancers than that in right-sided colon
333 cancers, and this higher expression level is associated with poor prognosis in right-sided colon cancers
334 (Xie et al., 2019). In gastric cancer, HOXB13 promotes cell migration and invasion by upregulating
335 PI3K/AKT/mTOR (Guo et al., 2021).

336 In the present study, IHC revealed high and universal HOXB13 expression in metaplastic
337 mucosa, including in both complete and incomplete subtypes; however, in normal mucosa, protein
338 expression was negligible (Figure 4C). These findings suggest that the HOXB13 regulon is
339 indispensable in the development of IM and that the phenotypic switch of LEFTY1+ possible stem cells
340 between gastric and metaplastic glands may require additional HOXB13 activation. Unlike in colonic
341 mucosa, the expression of HOXB13 was not observed in duodenal or iliac mucosa, suggesting that
342 metaplastic mucosa has similar characteristics to those of colonic mucosa (Figure 4C).
343 Regardless of *LEFTY1* expression, PG/Neck2 cells commonly showed high scores for SOX8
344 (Figure 4A; Figure S3A), for which an association with stomach biology has not been reported to date;
345 thus, further investigation of its function in the stomach is warranted. Meanwhile, LEFTY1+ADH+F cells
346 showed high scores for CDX1 and CDX2 (Figure 4A; Figure S3A), confirming that LEFTY1+ADH+F
347 cells are on the routes of differentiation of cells destined for the metaplastic lineage (Figure 2H). Fundic
348 gland-specific cells (i.e., chief and parietal cells) showed high SP5 activity (Figure S3A). Huggins et al.
349 (2017) reported that SP5 is a WNT target and negatively regulates WNT activity in human pluripotent
350 stem cells. We confirmed the specific expression of SP5 in fundic glands using RNA-ISH; thus, it
351 appears to be important in the development and/or maintenance of these glands (Figure 4D; Figure
352 S3B; see Methods).
353 Fazilaty et al. (2021) used scRNA-seq to show that embryonic enterocyte progenitor genes
354 were reactivated in the damaged enterocytes of both humans and mice. Given that the stomach and
355 intestine share common features, the gastric mucosa might also reactivate their progenitor programs
356 upon epithelial damage. Indeed, we found that metaplastic mucosa expressed *LEFTY1* and *HOXB13*,
357 both of which are embryonic genes (Kosaki et al., 1999; Ma et al., 2003), at higher levels than those in
358 normal pyloric or fundic mucosa. Moreover, in our pseudotime analysis, mature metaplastic mucosa
359 specifically expressed *APOA1*, one of the progenitor genes expressed in damaged colonic mucosa
360 (Figure 2B; Figure S3C), indicating that metaplastic enterocytes were similar to immature colonic

361 epithelium but not normal mucosa.

362

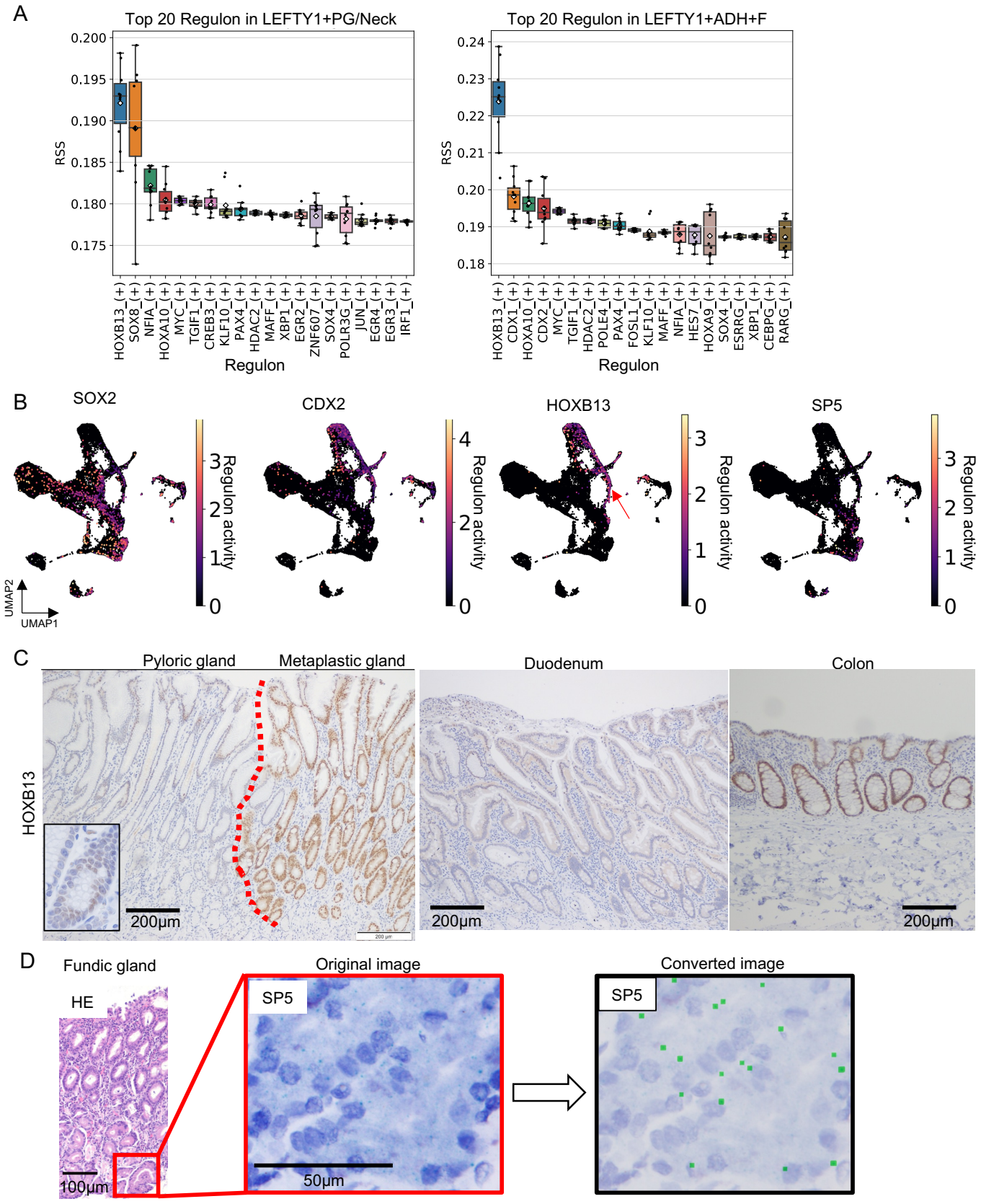
A
Top 20 Regulon in LEFTY1+PG/Neck
RSS
Regulon
HOXB13_(+)
SOX8_(+)
NFIA_(+)
HOXA10_(+)
MYC_(+)
TGIF1_(+)
CREB3_(+)
KLF10_(+)
PAX4_(+)
HDAC2_(+)
MAFF_(+)
XBP1_(+)
EGR2_(+)
ZNF607_(+)
SOX4_(+)
POLR3G_(+)
JUN_(+)
EGR4_(+)
EGR3_(+)
IRF1_(+)
Top 20 Regulon in LEFTY1+ADH+F
CDX1_(+)
CDX2_(+)
POLE4_(+)
FOSL1_(+)
HES7_(+)
HOXA9_(+)
ESRRG_(+)
CEBPG_(+)
RARG_(+)
B
SOX2
CDX2
HOXB13
SP5
Regulon activity
UMAP2
UMAP1
C
Pyloric gland
Metaplastic gland
Duodenum
Colon
HOXB13
200μm
D
Fundic gland
HE
100μm
Original image
SP5
50μm
Converted image

365 **Figure 4. Gene regulatory network analysis in epithelial cells revealed LEFTY1+ cell-specific**
366 **regulons.**

367 (A) LEFTY1+ cluster top 20 regulon specific scores calculated 10 times using pySCENIC. HOXB13
368 transcription factor showed highest scores commonly. LEFTY1+ADH+F showed relatively high
369 scores of CDX1 and CDX2, suggesting these cells are on the routes of differentiation of cells
370 destined for the metaplastic lineage. X-axis shows transcription factors.

371 (B) UMAP plot showing transcription activities of SOX2, CDX2, HOXB13, and SP5. High HOXB13
372 regulon activity was observed in the LEFTY1+ cell population (arrow) and metaplastic cells.
373 SOX2, CDX2, and SP5 regulon activity was high in the normal gastric cells, in the fundic gland
374 specific cells, in the metaplastic lineage cells, respectively.

375 (C) HOXB13 immunohistochemistry in the intestinal metaplasia, stomach, duodenum, and colon.
376 HOXB13 expression was observed in the metaplastic gland and genuine colonic mucosa. No
377 expression was observed in the duodenal mucosa. Inset: higher magnification of PG. Scale bar:
378 200 μm.

379 (D) RNA-ISH showing SP5 expression in the base of the fundic gland. Right: larger green pixels
380 converted computationally from original green signals (See methods for details).

381

382 **Fibroblasts**

383 As concluded by Higuchi et al. (2015), there are distinct differences in the stromal cells of the stomach
384 and intestinal mucosa; therefore, specific fibroblasts play key roles in maintaining epithelial homeostasis
385 in specific foci, and gastric fibroblasts are hypothesized to affect the developmental destinations of
386 gastric or metaplastic epithelia in the stomach. Previous studies on colorectal and gastric glands have
387 found that the proper compositions of fibroblasts and their secreting cytokines, including WNT, BMP, and
388 TGF-β ligands/inhibitors, were fundamental to the development and maintenance of digestive tissue
389 integrity (David et al., 2020; Koch, 2017; Wölffling et al., 2021; Zhang et al., 2020). In their scRNA-seq
390 study of the whole human body, Buechler et al. (2021) showed that various organ-specific fibroblasts
391 exist. However, global profiling of gastric-specific fibroblasts is lacking; thus, the characteristics of gastric
392 fibroblasts, as well as their similarities and differences to those in metaplastic mucosa, remain to be
393 elucidated. In the present study, we identified 5,225 fibroblasts, which were divided into 6 subclusters:
394 KLF+ cells (characteristic expression of *KLF4, SFRP1, SFRP2,* and *PI16*), CCL11+ cells (*CCL11,*
395 *ABCA8, APOE,* and *ADAM28*), PDGFR+ cells (*PLAT*, *POSTN*, *PDGFRA, BMP4,* and *WNT5A*), FibSmo
396 (Fibroblasts which express both fibroblastic and smooth muscle markers; He et al., 2020) (*HHIP*, *MYLK*,
397 and *ACTG2)*, smooth muscle cells (RERGL, ADIRF, MYH11, and *TAGLN*), and myofibroblasts (*RGS5*
398 and *CD36*) (Figures 5A and 5B; Figure S4A).

399 We compared our transcription profiling of stomach fibroblasts with that of the intestinal
400 fibroblasts in the cross-tissue fibroblast atlas (Buechler et al., 2021). Although PDGFRA^{hi} fibroblasts
401 were limited in intestinal tissues in the public database, our scRNA-seq data of stomach fibroblasts
402 included PDGFR+ fibroblasts (Figure 5B; Figure S4A). These PDGFR+ stomach fibroblasts and the
403 corresponding PDGFRA^{hi} intestinal fibroblasts in the public dataset commonly have specific expression
404 signatures of, for example, *PDGFRA*, *WNT5A,* and *BMP4*. In addition, the numbers of metaplastic
405 enterocytes and PDGFR+ fibroblasts were positively correlated in our single-cell dataset (Figure S4B),
406 suggesting that metaplastic epithelial cell and PDGFR+ fibroblasts interact with each other biologically to

407 maintain the metaplastic intestinal differentiation of the stomach.

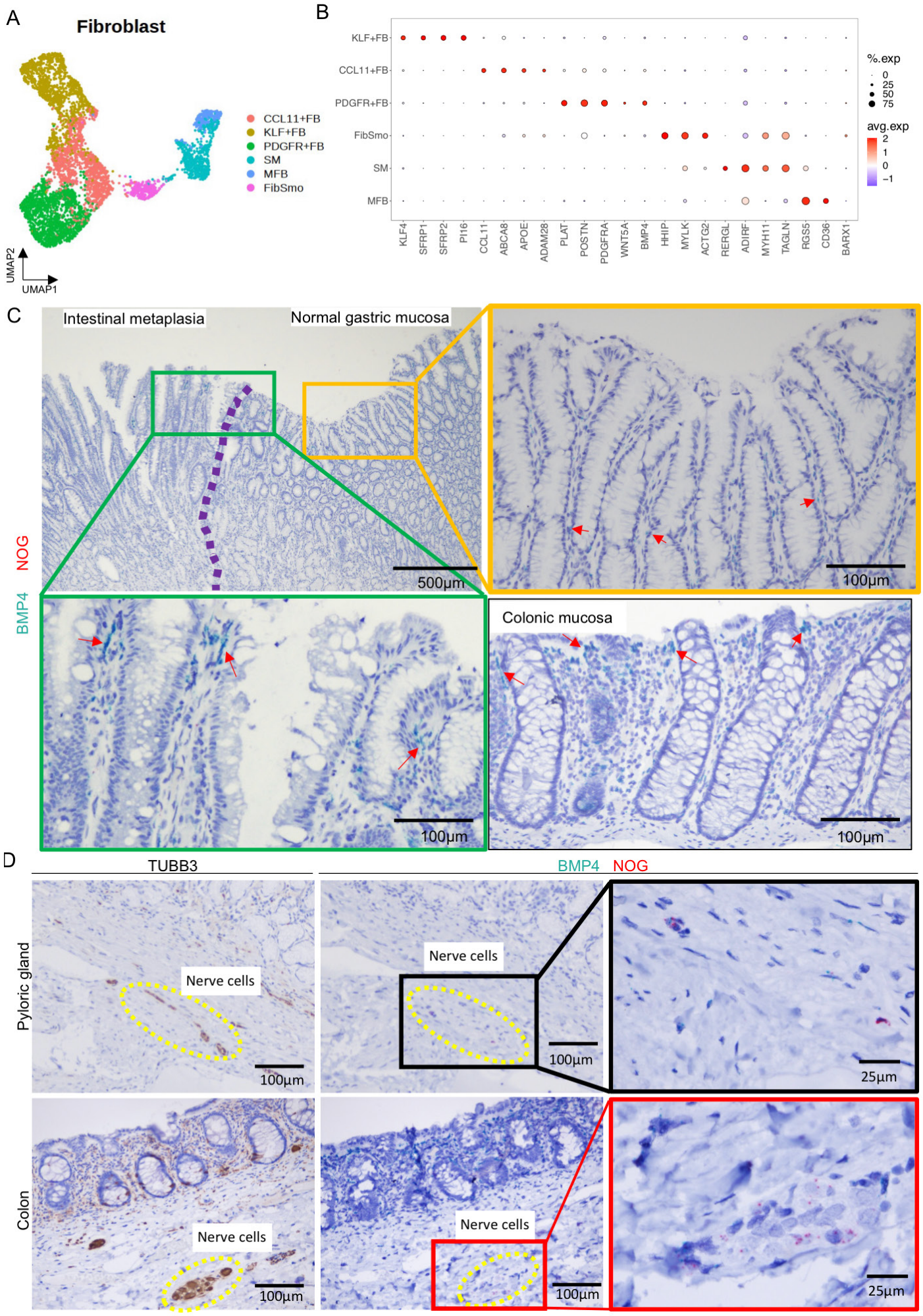
A
Fibroblast
CCL11+FB
KLF+FB
PDGFR+FB
SM
MFB
FibSmo
UMAP2
UMAP1
B
KLF+FB
CCL11+FB
PDGFR+FB
FibSmo
SM
MFB
KLF4
SFRP1
SFRP2
PI16
CCL11
ABCA8
APOE
ADAM28
PLAT
POSTN
PDGFRA
WNT5A
BMP4
HHIP
MYLK
ACTG2
RERGL
ADIRF
MYH11
TAGLN
RGS5
CD36
BARX1
%.exp
0
25
50
75
avg.exp
2
1
0
−1
C
Intestinal metaplasia
Normal gastric mucosa
500μm
100μm
NOG
BMP4
100μm
Colonic mucosa
100μm
D
TUBB3
BMP4 NOG
Pyloric gland
Nerve cells
100μm
Nerve cells
100μm
25μm
Colon
Nerve cells
100μm
Nerve cells
100μm
25μm

408

Figure 5. The increase of BMP4 expression in the fibroblasts that precedes the epithelial metaplastic transformation.

(A) UMAP showing the subclusters of 5,225 fibroblasts.

(B) Representative marker genes of fibroblast subclusters. Size and colors of circles show the percentage of cells expressing genes and average gene expression, respectively.

(C) RNA-ISH of BMP4. Green contour shows IM and the transitional region; yellow contour shows the pyloric gland. BMP4 expression in IM and the transitional region was similar to that in genuine colonic mucosa. The increase of BMP4 expression was observed in the metaplastic gland and normal gastric mucosa adjacent to IM. No NOG expression was observed in mucosal laminar propria both in the gastric and colonic mucosa. Arrows: BMP4 signals.

(D) Neuronal-specific TUBB3 IHC showing neuron cells in the submucosal region of the pyloric gland and colonic mucosa (Left). NOG expression was observed in the nerve cells both in the gastric and colonic mucosa (Right), whereas low BMP4 expression was observed. Yellow circles show nerve cells and the black contour shows RNA-ISH in high magnification.

Abbreviations: FB, fibroblasts; SM: smooth muscle; MFB: myofibroblasts.

To test the aforementioned hypothesis, we conducted RNA-ISH of *BMP4*, one of the signature genes among the PDGFR+ fibroblasts, and *NOG*, an intrinsic BMP antagonist (Zimmerman et al., 1996). In intestinal metaplastic mucosa, *BMP4*+ fibroblasts were more frequently discovered surrounding the metaplastic epithelial cells in the surface areas than in the gastric mucosa (Figure 5C; Figure S4C). The frequent existence of *BMP4*+ fibroblasts was also detected in normal gastric mucosa adjacent to metaplasia (Figure 5C; Figure S4C); however, in normal gastric mucosa distant from IM, *BMP4*+ fibroblasts were found infrequently (Figure 5C; Figure S4C). This suggests that composition changes in the population of specific fibroblasts occur earlier than the epithelial changes over the course of IM. In our ISH analysis, *BMP4* expression levels of the fibroblasts in the metaplastic mucosa of the stomach were comparable with those in genuine colonic mucosa (Figure 5C), suggesting that the physiology in BMP4-related tissue homeostasis was similar in metaplastic stomach glands and colorectal crypts, confirming by 3 stomach specimens including IM gland and 3 colon specimens. Also, we calculated the ratio of the BMP4 green signal area of RNA-ISH in the stroma from randomly selected five fields of the mucosal surface in normal gastric mucosa, transitional mucosa, intestinal metaplastic mucosa, and colonic mucosa. We found the monotonically increasing of BMP4 from normal gastric mucosa to metaplastic and colonic mucosa ($p= 0.001445$; Figure S4D). With these findings, we showed, for the first time, our hypothesis that the increase of BMP4 in the fibroblasts precede and may even induce IM. *NOG* expression was neither obvious in our scRNA-seq analysis nor was it observed in any cells in the mucosal layers of the stomach (Figure 5C; Figure S4A); however, neuron cell clusters, including ganglion cells, in submucosal layers expressed *NOG* in the stomach (Figure 5D). Drokhlyansky et al. (2020) showed that *NOG* is expressed in neuron cells in the colonic submucosa, but we are the first to report that neuron cells are the intrinsic source of *NOG* in the stomach. A previous study found that enteric neural crest cells promote antral stomach organoids (Eicher et al., 2022), suggesting the importance of nerve cells in the development and/or maintenance of epithelial cells. BMP signaling is known to induce *CDX2* expression in the gastric epithelium (Yoon et al., 2016), and NOG is essential for

451 establishing proper gastric organoids (Eicher et al., 2022; Zhang et al., 2020).

452 In our dataset, KLF+ fibroblasts (Figure 5A) characteristically expressed *SFRP1, SFRP2,*
453 *PI16,* and *CD34* (Figure 5B; Figure S4A), but no such fibroblasts existed in the intestine in the public
454 fibroblast atlas, suggesting that the KLF+ fibroblasts in our dataset are unique to the gastric mucosa.
455 RNA-ISH of SFRP1 showed KLF+ fibroblasts existed in the submucosa (Figure S5B). *CD34* is a
456 stemness-associated marker not only in hematopoietic cells but also in other mesenchymal cells
457 (Sydney et al., 2014); therefore, KLF+ gastric fibroblasts might have the potential to develop into other
458 fibroblast clusters. Additionally, KLF+ fibroblasts had the highest stemness score in our analyses (Figure
459 S4E), suggesting that these cells are tissue-resident fibroblasts with stemness features, which supports
460 our hypothesis that they have the potential to differentiate into other subtypes.

461 FibSmo cells (He et al., 2020), which express both fibroblastic and smooth muscle markers
462 (Figure 5B; Figure S4A), are an uncharacterized fraction. They are distributed in the midpoint between
463 myofibroblasts and other characteristic fibroblasts with signature gene expression, such as that of
464 *PDGFRA* and *KLF4* (Figure 5A), suggesting that FibSmo cells play a unique role among the fibroblast
465 lineages. FibSmo cells specifically express high levels of *HHIP* (hedgehog interaction protein; Figure 5B;
466 Figure S4A), which functions as a regulatory component of the Hedgehog signaling pathway, a pathway
467 required in the development of the normal stomach in both mice and human (El-Zaatari et al., 2009; Katoh
468 and Katoh, 2006). We also found that expression of *BARX1*, which encodes a stomach fibroblast-specific
469 transcription factor, was highest in FibSmo cells (Figure 5B; Figure S4A). Kim et al. (2005) found that
470 *Barx1*-knockout mice did not develop a normal stomach and that intestinal markers were activated;
471 therefore, *BARX1+* stomach fibroblasts may play a key role in normal gastric development. We performed
472 RNA-ISH to confirm the stomach-specific expression of *BARX1* as well as the coexpression of *HHIP* in
473 *BARX1+* fibroblasts, finding that *BARX1* expression in fibroblasts occurred in the lamina propria of the
474 pyloric and fundic gland mucosa, indicating that *BARX1* interacted with epithelial cells through its
475 downstream genes (Figure 6A). In contrast, *BARX1+* fibroblasts were not observed in genuine colonic

476 and small intestinal mucosa (Figure 6A); however, in the intestinal metaplastic mucosa of the stomach,
477 the frequencies of *BARX1*+ fibroblasts were comparable to those detected in the gastric mucosa (Figure
478 6A). We also found clear coexpression of *BARX1* and *HHIP* in parts of the stomach fibroblasts, although
479 *BARX1* expression was detected more broadly than *HHIP* expression in fibroblasts (Figure 6A). Based on
480 these findings, we confirm the existence of a unique subset of stomach-specific fibroblasts, i.e.,
481 *BARX1*+/*HHIP*+ FibSmo fibroblasts, which warrant further functional investigation in relation to the
482 development of the stomach and IM.
483
484
485

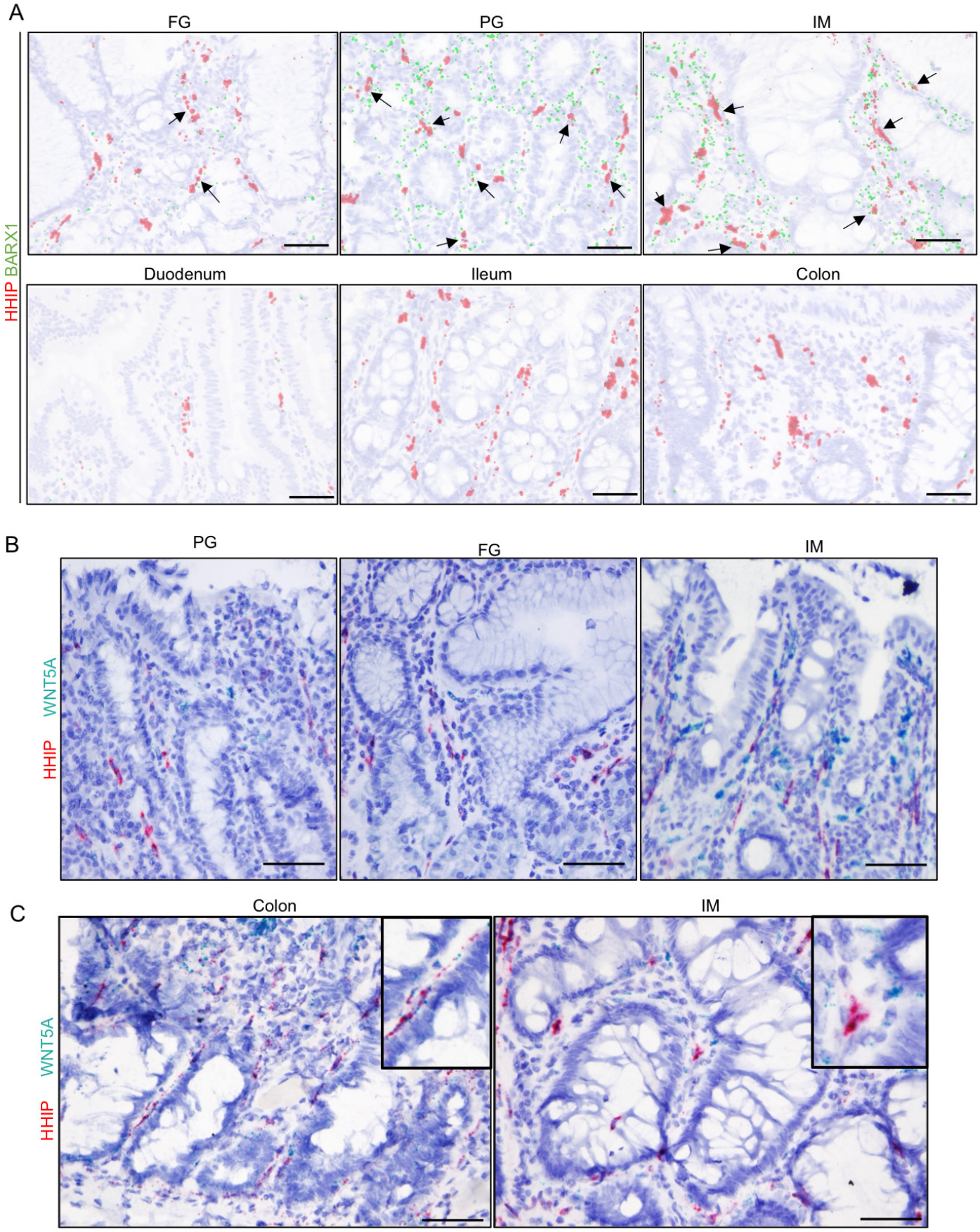
A
FG
PG
IM
HHIP BARX1
Duodenum
Ileum
Colon
B
PG
FG
IM
HHIP WNT5A
C
Colon
IM
HHIP WNT5A

486

487

488 **Figure 6. Unique spatial distribution of BARX1, HHIP, and WNT5A-positive fibroblasts in gastric**
489 **mucosa.**

490 (A) HHIP and BARX1 RNA-ISH in each gland or tissue. HHIP and BARX1 coexpression was
491 observed in gastric mucosa including IM (arrows). BARX1 expression was not observed in small
492 intestinal and colonic mucosa, as expected. BARX1 blue signals and HHIP red signals were
493 converted to enlarged green and red pixels, respectively, for ease of detection, as explained in
494 Figure 4D. Arrows: Coexpression of HHIP and BARX1. Scale bar: 50 μm.

495 (B) WNT5A and HHIP RNA-ISH in each tissue. WNT5A was highly expressed in IM relative to its
496 expression in normal mucosa. WNT5A expression was more observed in the surface area and in
497 the just behind epithelial cells, whereas HHIP expression was distant from epithelial cell layers.
498 Scale bar: 50 μm.

499 (C) WNT5A and HHIP RNA-ISH in the colonic mucosa and metaplastic mucosa. WNT5A and HHIP
500 coexpression was observed in colonic mucosa, whereas not in IM. Inset shows higher
501 magnification of each region. Scale bar: 50 μm.

502

503 *BARX1* is reported to induce the expression of secreted frizzled-related protein (SFRP), which
504 promotes differentiation of the stomach epithelium by blocking local WNT signaling during the
505 developmental stage (Kim et al., 2005). Interestingly, *BARX1* was expressed at measurable levels in all
506 fibroblast subtypes in our samples, but SFRP expression was mostly limited in the KLF+ fibroblasts
507 (Figure 5B; Figure S4A). RNA-ISH revealed that SFRP1 and BARX1 were not coexpressed in stomach
508 fibroblasts, suggesting that BARX1 does not induce SFRP1 in the fibroblasts of the adult stomach
509 (Figure S5A). Additionally, SFRP+ fibroblasts were observed only in the submucosal layer of the
510 stomach, unlike in the colon mucosa in which SFRP was expressed by fibroblasts in the mucosal layer
511 (Figures S5B and S5C). Therefore, we might postulate the hypothesis that insufficient WNT inhibition by
512 SFRPs in intestinal metaplastic mucosa, unlike in normal colorectal mucosa, could be one of possible
513 causes of unregulated malignant transformation of the metaplastic stomach epithelia.
514 Our scRNA-seq analysis confirmed that some fractions of stomach fibroblasts are sources of
515 cytokines that regulate WNT or Hedgehog signaling, i.e., the PDGFR+ fibroblasts and FibSmo cells
516 express *WNT5A*, an inhibitor of canonical WNT signaling, and *HHIP*, respectively (Figure 5B). Several
517 studies have suggested that the physical distributions of fibroblasts and resultant local cytokine milieus
518 are vital to the proper development of digestive organs (Ormestad et al., 2006; Roy et al., 2016;
519 Shinohara et al., 2010). SHH or IHH mutant stomachs show abnormal morphology or expression of
520 intestinal markers (Thompson et al., 2018); therefore, the pan-Hedgehog inhibitor HHIP has important
521 functions in the development and homeostasis of the stomach. Thus, we speculate that the spatial
522 distributions of specific stomach fibroblast subtypes play important roles in the tissue architectures of
523 gastric and metaplastic mucosa. Our ISH analysis of *WNT5A* in the stomach and colon tissues revealed
524 that *WNT5A* was expressed in both gastric and metaplastic mucosa, mainly in the surface areas, as
525 reported previously in relation to colonic mucosa (Gregorieff et al., 2005) (Figures 6B and 6C). *WNT5A*
526 expression was more intense in the metaplastic regions than in the pyloric or fundic mucosa, consistent
527 with *BMP4* expression (Figure 6B). *HHIP* expression was also observed broadly in both gastric and

528 metaplastic mucosa; however, in contrast to *WNT5A*, *HHIP*+ fibroblasts were not limited to the surface
529 areas but found at broader depths of the stomach mucosa (Figure 6C). Intriguingly, the close lining of
530 *WNT5A*+ fibroblasts just behind the epithelial cells was frequently observed throughout the stomach
531 mucosa (Figure 6B). Conversely, *HHIP*+ fibroblasts were distributed in stromal spaces at distances from
532 the epithelial cell layers (Figures 6A and 6B). Therefore, WNT5A seems to act locally, i.e., only on the
533 neighboring epithelial cells, whereas HHIP acts more broadly by spreading to distant epithelial cells.
534 Notably, although *HHIP+/WNT5A*+ double-positive fibroblasts were frequently observed in colonic
535 mucosa, such coexpression of *HHIP* and *WNT5A* was not found among stomach fibroblasts, regardless
536 of gastric or metaplastic conditions (Figure 6C). In conclusion, although gastric and colonic fibroblasts
537 share some characteristics, they also harbor their own specific features and probably have distinct
538 functions.

539 We performed gene regulatory network analysis on the fibroblasts (Figure S5D), finding that
540 forkhead box transcription factors play a role in their biology. Specifically, FOXF1, FOXF2, and FOXL1
541 transcription activities were upregulated in PDGFR+ fibroblasts as well as FibSmo cells. Correlations
542 among *FOXF1, FOXF2*, and *BMP4* expression and between *FOXL1* and WNT expression have been
543 reported in murine colon fibroblasts (Kaestner, 2019; Ormestad et al., 2006). Therefore, FOXF1/2+ and
544 FOXL1+ fibroblasts are apparently important for regulating stomach homeostasis and metaplastic
545 transformation.

546

547 **Immune and endothelial cells**

548 We obtained 71,594 B and plasma cells, including 41,544 plasma cells (with characteristic expression of
549 immunoglobulins, such as *IGHG1, IGHA1,* and *IGKC*), 29,816 B cells (*MS4A1* and *HLA-DRA*), and
550 15,778 T lymphocytes, with 5 subclusters: CD8 T cells (*CD8A* and *CD8B*; including the GZMK+ CD8
551 subtype), CD4+CTLA4+T cells (*CD4, PDCD1, CTLA4,* and *FOXP3*), CD4+CD40LG+T cells (*CD4* and
552 *CD40LG*), and γδ T cells (*TRDC* and *TRGC1*) (Figures S6A, S6B, S6E, and S6F). Notably, the

553 proportion of γδ T cells was higher in intestinal metaplastic mucosa compared with that in stomach
554 mucosa (Figure S4B), consistent with the study of Romi et al. (2011), who reported a positive correlation
555 between the number of γδ T cells and *Helicobacter*-associated gastritis. We obtained 2,002 myeloid
556 cells with clusters of dendritic cells, monocytes/neutrophils, and macrophages (Figures S6C and S6G).
557 Conventional M1/2 macrophages or CD14/CD16 monocyte clusters were not identified, consistent with
558 a scRNA-seq atlas of tumor-associated myeloid cells (Cheng et al., 2021), which showed that the
559 myeloid cells have complex phenotypes rather than classical M1 and M2 phenotypes.
560 In total, 3,028 endothelial cells were identified with 4 subtypes: 1,950 PLVAP+ endothelial
561 cells, 748 ACKR1+ cells, 243 FN1+ cells (characteristic for *DEPP1, FN1,* and *CXCL2*), and 130
562 lymphatic endothelial cells (*CCL21* and *LYVE1*) (Figures S6D and S6H). FN1+ cells seemed to be
563 arteries, whereas other endothelial cells were considered venous capillaries based on the expression of
564 EFNB2 and EPHB4 (Kania and Klein, 2016) (Figure S6H). Our IHC analysis showed that ACKR1+
565 endothelial cells existed in vessels at deeper regions of the stomach mucosa, whereas PLVAP+
566 endothelial cells constructed vessels in much wider layers of the stomach mucosa, regardless of
567 fundic/pyloric and metaplastic mucosa (Figures S6I–K).
568
569 **Cell–cell communication analysis of epithelial cells and stromal cells**
570 Using scRNA-seq analysis, we identified diverse stomach cells in both the physiological and metaplastic
571 mucosa. Various signaling interactions between these cells through cytokines, chemokines, and direct
572 ligand–receptor bindings play important roles in the maintenance of tissue homeostasis in the stomach;
573 thus, we sought to elucidate the cell–cell communication (CCC) networks to deepen our understanding
574 of the cellular diversity of the stomach. CCC analysis was performed by combining a gene expression
575 matrix from our scRNA-seq data with known datasets of ligand–receptor complexes (Jin et al., 2021).
576 Notably, epithelial cell lineages were one of the most enriched cell types from and to which a great
577 diversity of CCC was interconnected (Figure 7A). In addition, we found many more interactions were

578 observed among enterocytes, fibroblasts, and myeloid cells in severe IM, compared with nonsevere IM
579 status (Figures S7A and S7B), suggesting nonepithelial microenvironment contributes development
580 and/or maintenance of epithelial intestinal metaplasia. From the CCC detected around epithelial cells,
581 we focused on LEFTY1+ cells as models for investigating the possible mechanisms by which stem cell
582 properties are maintained (Figure 7A). As shown in Figure S2B, the LEFTY1+ cells also expressed
583 CD44, another known stem cell marker (Ye et al., 2018). CCC analysis revealed that a signaling network
584 of macrophage migration inhibitory factor (MIF), a ligand of the CD74+CD44 complex and
585 CD74+CXCR4 complex (Becker-Herman et al., 2021; Shi et al., 2006), had characteristic features, i.e.,
586 many of MIF–(CD74+CD44) and MIF–(CD74+CXCR4) interactions are mediated by LEFTY1+ cells
587 among all the cell types identified in gastric mucosa (Figure 7B). We conclude, therefore, that LEFTY1+
588 epithelial cells function as a hub of cellular communications via CD44 networks. Given that LEFTY1+
589 cells also show the highest expression of MIF among epithelial cell types (Figure S8A), CD44, and its
590 communication networks potentially function in an autocrine manner in these cells. The multilayered
591 interactions of LEFTY1+ cells with various other cells, including epithelial cell types, support our
592 hypothesis that LEFTY1+ epithelial cells compose a possible stem cell cluster. CD74 is another
593 communication partner of CD44, and the CD74–CD44 complex functions to prevent apoptosis and
594 maintain stem cell properties (Becker-Herman et al., 2021; Gore et al., 2008; Shi et al., 2006). In
595 contrast to other cell types, we found that a CD44 and CD74 coexpression pattern existed in LEFTY1+
596 epithelial cells (Figure S8B), providing further evidence that LEFTY1+ possible stem cells function in
597 concert with the CD44 network.

598 As we reported, PDGFR+ fibroblasts expressing BMP4 and/or WNT5A showed characteristic
599 properties in the stomach mucosa, specifically in the intestinal metaplastic mucosa. Additionally, a CCC
600 comparison between severe and nonsevere IM revealed the specific enrichment of NRG signaling in
601 severe IM (Figures S7A and S7B). We also found that PDGFR+ fibroblasts expressed *NRG1*, the
602 product of which is neuregulin-1 (NRG1), characteristically (Figure 7C; Figure S8C). In our CCC

603 analysis of the NRG1 network, PDGFR+ fibroblasts interacted with various epithelial cells, including
604 LEFTY1+PG/Neck cells, LEFTY1+ADH1+F cells, and enterocytes, all of which expressed ERBB3, a
605 receptor for NRG1 (Meyer and Birchmeier, 1995) (Figure S8D). NRG1–ERBB2/ERBB3 signaling is
606 known to act against apoptosis to preserve differentiation in human trophoblasts (Fock et al., 2015), and
607 *NRG1* drives intestinal stem cells to proliferate and regenerate in damaged epithelia (Jardé et al., 2020).
608 Over the course of IM in the damaged stomach, stomach epithelial cells receive NRG1 signals from
609 fibroblasts and eventually differentiate into metaplastic enterocytes. Our CCC analysis is consistent with
610 our spatial distribution analysis of the PDGFR+ fibroblasts (Figures 5C and 6B), i.e., the migration of
611 PDGFR+ stromal fibroblasts precedes the development of intestinal metaplastic mucosa. Taken
612 together, our CCC analyses show that PDGFR+ fibroblasts and secreted NRG1 play important roles in
613 the development of intestinal metaplastic mucosa.

614 Interactions between EPHB2 in LEFTY1+ PG/Neck cells and EFNB2 in various epithelial and
615 FN1+ endothelial cells were of interest in our CCC analysis (Figure 7D; Figure S8D). Eph–ephrin
616 complexes have a distinct feature of generating bidirectional signals that affect both Eph-expressing and
617 ephrin-expressing cells. Eph–ephrin interactions generate repulsive reactions, which play important
618 roles in the formation of cell clusters and stripe patterns in organogenesis, including in somite and
619 neuronal differentiation (Kania and Klein, 2016; Pitulescu and Adams, 2010). In murine intestinal
620 mucosa, stem cells, during their differentiation into proliferation progenitors, gradually lose *Ephb2*
621 expression, whereas *Efnb2* expression is highest at the villous–crypt boundary (Kania and Klein, 2016).
622 In our scRNA-seq dataset, surface epithelial cells, such as metaplastic enterocytes and ADH1+GKN1-F
623 cells, showed the highest levels of *EFNB2* expression (Figures S8D and S8E). Using IHC, we showed
624 that EPHB2 was only positive in the crypt base of IM, whereas EFNB2 was positive in other regions of
625 IM and the superficial region of gastric mucosa (Figure S8F). This confirms that the function of Eph–
626 ephrin repulsion in intestinal metaplastic mucosa is similar to that in colorectal crypts; however, this
627 interaction was not observed in stomach mucosa. This implies that different combinations of Eph–ephrin

628 interactions or unknown regulation mechanisms might play some roles in stomach glands.

629 Although our CCC analysis did not identify clear enrichment of the major signaling pathways of
630 BMP or WNT between epithelial cells and fibroblasts, the spatial distribution of WNT5A+ fibroblasts
631 (Figures 6B and 6C) suggested that interesting cellular interactions possibly occur around WNT/BMP.
632 According to RNA-ISH analysis, WNT5A+ fibroblasts were mainly found in the surface area of stomach
633 mucosa (Figures 6B and 6C); however, following closer observations, we found that WNT5A+ fibroblasts
634 were also found in line with LEFTY1+ possible stem cells at the crypt bases of IM (Figure S8G). This
635 close physical interaction between LEFTY1+ cells and WNT5A+ fibroblasts was specific to metaplastic
636 mucosa, i.e., it was not detected in pyloric glands (Figure S8G). LEFTY1 functions as a TGF-β inhibitor
637 (Zabala et al., 2020), whereas WNT5A can potentiate as a TGF-β signaling to control stem cell
638 properties and construct regenerative crypts (Miyoshi et al., 2012); thus, LEFTY1 and WNT5A might
639 work in concert in relation to IM in the stomach. We reported that LEFTY1 IHC revealed two different
640 protein expression patterns; the intense dot pattern indicates the directional secretion of protein into the
641 stromal environment, supporting its biological interaction with the local cytokines/receptors around the
642 stomach gland, such as BMP4 or WNT5A.
643

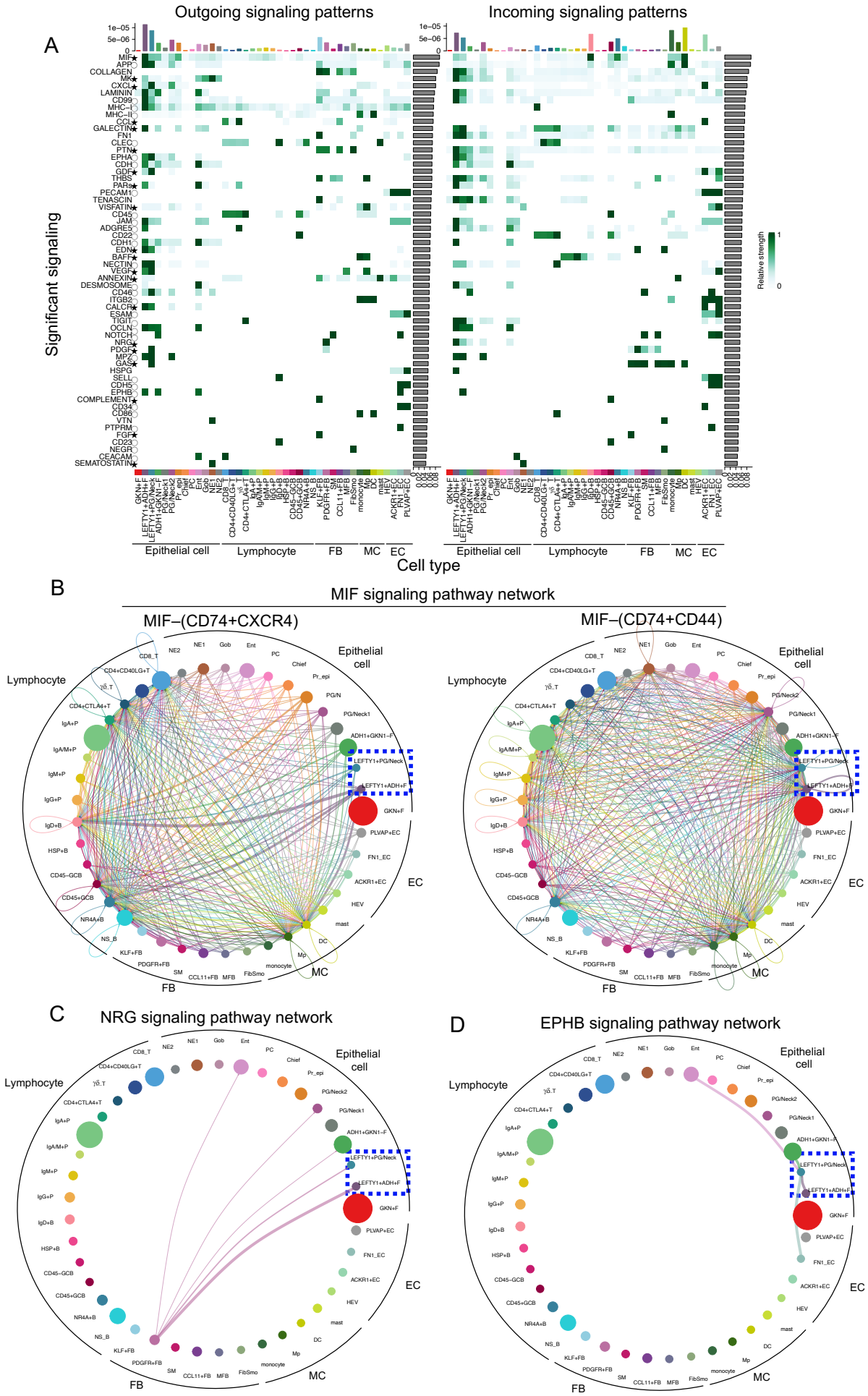
A
Outgoing signaling patterns
Incoming signaling patterns
Significant signaling
Relative strength
Epithelial cell
Lymphocyte
FB
MC
EC
Cell type
B
MIF signaling pathway network
MIF–(CD74+CXCR4)
MIF–(CD74+CD44)
C
NRG signaling pathway network
D
EPHB signaling pathway network

644

Figure 7. Global view of cell–cell interactions among each cell clusters identified in gastric mucosa, and detailed analysis for focused interactions.

(A) Overview of each cell-type and signaling patterns showing that LEFTY1+ cells were centered in the communication network. Top bar plots showing the sum of the communication probability calculated by cellchat library for each cell type. Right bar plots showing the proportion of the contribution in each signal to the total. Heatmaps showing relative strength for each cell type in each signaling. *: secreting signals; O: cell–cell contact; no symbol: extracellular matrix. Jin et al. (2021) provide the signal ligand and receptor pair details.

(B–D) Focused interaction network performed by CCC analysis. The circle size of each cluster reflects on the number of cells in each cluster. The thickness of the flow indicates the communication probability. Arrows on outgoing signals and the cluster circles are the same color.

(B) Macrophage migration inhibitory factor (MIF) signaling pathway network showing that LEFTY1+ cells expressed both the ligand and receptor. MIF interacts with the CD74+CXCR4 and CD74+CD44 complexes.

(C) Neuregulin (NRG) signaling pathway network showing that PDGFR+FB expressed the ligand, NRG1, and enterocytes and that its progenitor cells expressed its receptors ERBB2 and ERBB3.

(D) EPHB signaling pathway network showing that LEFTY1+PG/Neck expressed EPHB2 and other mature enterocytes expressed its ligand EFNB2.

664 **Gene set enrichment analysis of the cells identified via scRNA-seq**

665 To investigate the functional status in each cellular lineage, gene set enrichment analysis was performed
666 for various cell clusters. Some known gene sets identified by Busslinger et al. (2021) with parietal, chief,
667 and gastric neck cell properties were clearly enriched in our parietal, chief, and neck cell populations,
668 respectively, confirming the robustness of our analysis (Figure S9A). Metaplastic enterocytes and
669 LEFTY1+ cells were enriched with gene sets for adipogenesis, fatty acid metabolism, glycolysis,
670 oxidative phosphorylation, and reactive oxygen species pathways. Moreover, a gene set of the MYC
671 pathway "HALLMARK_MYC_TARGETS_V1" was characteristically enriched in LEFTY1+ cells together
672 with multiple gene sets associated with stem cell properties (Figure S9B). In general, quiescent stem
673 cells use glycolysis within a hypoxic niche but context-dependently proliferate and differentiate under
674 other conditions, switching to oxidative phosphorylation (Shyh-Chang and Ng, 2017). The enrichments
675 of metabolic-related gene features and MYC pathway activation suggest that the LEFTY1+ epithelial
676 population, a cluster of a possible stomach stem cells, has a complex and dedicated metabolic
677 regulation pathway; thus, additional studies are required to clarify these complex dynamics.

678

679 **Hedgehog signal regulation in gastric mucosa**

680 Hedgehog signaling is an important factor that regulates the development and maintenance of
681 gastrointestinal tracts (Dimmler et al., 2003; Katoh and Katoh, 2006; Thompson et al., 2018), but it was
682 not a focus of the above-reported analysis. A previous study showed that *SHH* mutant mice exhibited
683 intestinal transformation of the stomach (Ramalho-Santos et al., 2000). Additionally, recurrent *MALAT1-*
684 *GLI1* fusion was reported in plexiform fibromyxoma and gastroblastoma, stomach-specific mesenchymal
685 and mixed epithelial–mesenchymal tumors (Graham et al., 2017), suggesting the importance of
686 Hedgehog signaling in the stomach, especially mesenchyme. Both SHH and IHH from epithelial cells
687 are known to activate FOXL1-mediated BMP4 expression in mesenchymal cells (Katoh and Katoh,
688 2006). In our dataset, SHH expression was limited in gastric lineage, whereas IHH was expressed in

689 both epithelial cells of gastric lineages and metaplastic lineages, respectively (Figure S10A). Although,
690 to our knowledge, studies are lacking on the differential biological functions of *SHH* and *IHH* in the gut,
691 *SHH* and *IHH* may function differently during tissue homeostasis of gastric and metaplastic mucosa. The
692 Hedgehog receptors *PTCH1* and *PTCH2* were expressed occasionally in some PG/Neck1 cells and
693 PDGFR+ fibroblasts, and the downstream effectors of Hedgehog, *GLI1*, *GLI2*, and *GLI3*, were
694 expressed modestly in diverse subtypes of epithelial cells and fibroblasts (Figure S10A). Thus,
695 hedgehog pathways might play important roles in the development and maintenance of stomach
696 tissues. Of the fibroblasts, both FibSmo and PDGFR+ cells expressed *PTCH1*, whereas only FibSmo
697 cells expressed *HHIP*, a negative regulator of the hedgehog pathway (Figures S4A and S10A). *PTCH1*
698 and *HHIP* expression can be induced by a downstream hedgehog signal as a component of negative
699 feedback machinery (Katoh and Katoh, 2006); thus, at least FibSmo fibroblasts seem to exhibit active
700 hedgehog pathways, presumably through the receipt of SHH/IHH from epithelial cells. Considering
701 normal gastric cells and metaplastic enterocytes express *SHH* and *IHH*, respectively, and BMP4
702 expression is regulated by hedgehog signaling, and BMP4-secreting fibroblasts increase in IM gland, we
703 assume that both SHH and IHH affect the balance between BMP and hedgehog signaling, but the
704 suitable ratio of these components may differ between gastric and intestinal metaplastic mucosa. We
705 hypothesized that, once the balance of hedgehog and BMP signaling in the stomach is disturbed by
706 chronic inflammation or other stimuli, tissues may experience a perturbed cytokine environment that
707 induces IM.
708

709 **Upregulation of metabolite-related genes in possible stem cells**

710 In addition to our gene set enrichment analysis, other studies have identified the biological links between
711 stem cell features and the metabolic activity of various pathways (Carey et al., 2015; Cheng et al., 2019;
712 Tischler et al., 2019). Specifically, Cheng et al. (2019) suggested that HMGCS2 and its metabolite β-
713 hydroxybutyrate play important roles in maintaining epithelial stemness, inhibiting histone deacetylase

714 (HDAC), and reinforcing NOTCH signaling in the intestine. They also reported that *HMGCS2* is
715 expressed at higher levels in the *LGR5*+ stem cells of the colon. In our dataset, *HMGCS2* and HDACs
716 (*HDAC1*, *HDAC2*, and *HDAC3*) were clearly enriched in LEFTY1+ cells (Figure S10B), indicating that
717 these cells are possible stomach stem cells, consistent with the findings of the aforementioned studies.
718 Moreover, we found that *IDH1* and *IDH2* were enriched in LEFTY1+ cells (Figure S10C). α-
719 Ketoglutarate is a well-established metabolite of the IDHs, and intracellular α-ketoglutarate is known to
720 maintain the stemness of embryonic stem cells (Carey et al., 2015); thus, the enrichment of IDHs in
721 LEFTY1+ cells is also indicative of their stemness properties.
722

723 **CONCLUSION**

724 In this study, we constructed the largest ever stomach cell atlas at a single-cell resolution. This data
725 constitutes a unique resource that will be used in a variety of investigations on stomach development
726 and disease pathology. Combined with sophisticated bioinformatics analyses, we identified a novel
727 candidate common stem cell population in the adult stomach, i.e., the LEFTY1+ cell cluster, and
728 uncovered the skewed and characteristic distributions of specific subtypes of fibroblasts in the
729 ecosystems of normal and metaplastic stomach mucosa. In addition, our CCC analysis revealed that
730 LEFTY1+ is the most enriched population in both outgoing and incoming signaling patterns, supporting
731 the hypothesis that the LEFTY1+ population plays a pivotal role in the maintenance of gastric epithelial
732 integrity. Gene set enrichment analysis and focused metabolic gene expression analyses confirmed and
733 further suggested the complex dynamics of stem cell metabolism. Overall, our study provides novel and
734 unexpected findings related to the normal and metaplastic ecosystems of the stomach that warrant
735 further developmental and cancer research, including the expansion of our dataset with additional
736 scRNA-seq human cell atlases, such as those of other digestive organs and gastric cancers.
737

738 **STAR METHODS**

Detailed methods are provided in the online version of this paper and include the following:

- KEY RESOURCES TABLE
- RESOURCE AVAILABILITY
  - Lead contact
- EXPERIMENTAL MODELS AND SUBJECT DETAILS
  - Human specimens
- METHOD DETAILS
  - Single-cell RNA sequencing
  - Data preprocessing for scRNA-seq
  - Clustering, visualization, and cell annotation
  - Annotation of IM status
  - Transcriptional entropy and trajectory analysis
  - Gene regulatory network and cell–cell interaction analysis
  - Hematoxylin and eosin staining
  - Immunohistochemistry
  - RNAScope
  - Signal magnification of RNAScope

ACKNOWLEDGMENTS

We thank Enago (www.enago.jp) for the English language review. Figure illustrations were created in part using Biorender.com. This study was supported by the AMED Practical Research for elucidation of genomic diversity and identification of clinical intervention for gastric cancers with a focus on humoral immunity (grant number JP 21cm0106551 to S.I.).

AUTHOR CONTRIBUTIONS

Conceptualization, S.I.; Experiments, A.T., H.K., M.K., A.Y., and T.O.; Computational Analysis, D.K. and A.T.; Resources, H.A., Y.S., and T.U.; Writing, A.T., H.K., D.K., M.K., and S.I.; Supervision, S.I.

REFERENCE

768 1. Aibar, S., González-Blas, C.B., Moerman, T., Huynh-Thu, V.A., Imrichova, H., Hulselmans, G.,
769 Rambow, F., Marine, J.C., Geurts, P., Aerts, J., et al. (2017). SCENIC: Single-cell regulatory
770 network inference and clustering. Nat. Methods *14*, 1083–1086.
771 2. Alarcón-Millán, J., Martínez-Carrillo, D.N., Peralta-Zaragoza, O., and Fernández-Tilapa, G. (2019).
772 Regulation of GKN1 expression in gastric carcinogenesis: A problem to resolve (Review). Int. J.
773 Oncol. *55*, 555–569.
774 3. Almeida, R., Silva, E., Santos-Silva, F., Silberg, D.G., Wang, J., De Bolós, C., and David, L. (2003).
775 Expression of intestine-specific transcription factors, CDX1 and CDX2, in intestinal metaplasia and
776 gastric carcinomas. J. Pathol. *199*, 36–40.
777 4. Aran, D., Looney, A.P., Liu, L., Wu, E., Fong, V., Hsu, A., Chak, S., Naikawadi, R.P., Wolters, P.J.,
778 Abate, A.R., et al. (2019). Reference-based analysis of lung single-cell sequencing reveals a
779 transitional profibrotic macrophage. Nat. Immunol. *20*, 163–172.
780 5. Bais, A.S., and Kostka, D. (2020). Scds: Computational annotation of doublets in single-cell RNA
781 sequencing data. Bioinformatics *36*, 1150–1158.
782 6. Becker-Herman, S., Rozenberg, M., Hillel-Karniel, C., Gil-Yarom, N., Kramer, M., Barak, A., Sever,
783 L., David, K., Radomir, L., Lewinsky, H., et al. (2021). CD74 is a regulator of hematopoietic stem
784 cell maintenance. PLoS Biol. *19*, 1–24.
785 7. Buechler, M.B., Pradhan, R.N., Krishnamurty, A.T., Cox, C., Calviello, A.K., Wang, A.W., Yang,
786 Y.A., Tam, L., Caothien, R., Roose-Girma, M., et al. (2021). Cross-tissue organization of the
787 fibroblast lineage. Nature *593*, 575–579.
788 8. Busslinger, G.A., Weusten, B.L.A., Bogte, A., Begthel, H., Brosens, L.A.A., and Clevers, H. (2021).
789 Human gastrointestinal epithelia of the esophagus, stomach, and duodenum resolved at single-cell
790 resolution. Cell Rep. *34*.

791 9. Cao, J., Spielmann, M., Qiu, X., Huang, X., Ibrahim, D.M., Hill, A.J., Zhang, F., Mundlos, S.,
792 Christiansen, L., Steemers, F.J., et al. (2019). The single-cell transcriptional landscape of
793 mammalian organogenesis. Nature *566*, 496–502.
794 10. Carey, B.W., Finley, L.W.S., Cross, J.R., Allis, C.D., and Thompson, C.B. (2015). Intracellular α-
795 ketoglutarate maintains the pluripotency of embryonic stem cells. Nature *518*, 413–416.
796 11. Cheng, C.-W., Biton, M., Haber, A.L., Gunduz, N., Eng, G., Gaynor, L.T., Tripathi, S., Calibasi-
797 Kocal, G., Rickelt, S., Butty, V.L., et al. (2019). Ketone Body Signaling Mediates Intestinal Stem Cell
798 Homeostasis and Adaptation to Diet. Cell *178*, 1115-1131.e15.
799 12. Cheng, S., Li, Z., Gao, R., Xing, B., Gao, Y., Yang, Y., Qin, S., Zhang, L., Ouyang, H., Du, P., et al.
800 (2021). A pan-cancer single-cell transcriptional atlas of tumor infiltrating myeloid cells. Cell *184*,
801 792-809.e23.
802 13. Choi, M.Y., Romer, A.I., Wang, Y., Wu, M.P., Ito, S., Leiter, A.B., and Shivdasani, R.A. (2008).
803 Requirement of the Tissue-Restricted Homeodomain Transcription Factor Nkx6.3 in Differentiation
804 of Gastrin-Producing G Cells in the Stomach Antrum. Mol. Cell. Biol. *28*, 3208–3218.
805 14. David, M.B., Valenta, T., Fazilaty, H., Hausmann, G., and Basler, K. (2020). Distinct populations of
806 crypt-associated fibroblasts act as signaling hubs to control colon homeostasis. PLoS Biol. *18*, 1–
807 20.
808 15. Dimmler, A., Brabletz, T., Hlubek, F., Häfner, M., Rau, T., Kirchner, T., and Faller, G. (2003).
809 Transcription of Sonic Hedgehog, a Potential Factor for Gastric Morphogenesis and Gastric Mucosa
810 Maintenance, Is Up-regulated in Acidic Conditions. Lab. Investig. *83*, 1829–1837.
811 16. Drokhlyansky, E., Smillie, C.S., Van Wittenberghe, N., Ericsson, M., Griffin, G.K., Eraslan, G.,
812 Dionne, D., Cuoco, M.S., Goder-Reiser, M.N., Sharova, T., et al. (2020). The Human and Mouse
813 Enteric Nervous System at Single-Cell Resolution. Cell *182*, 1606-1622.e23.
814 17. Edenberg, H.J., and McClintick, J.N. (2018). Alcohol Dehydrogenases, Aldehyde Dehydrogenases,
815 and Alcohol Use Disorders: A Critical Review. Alcohol. Clin. Exp. Res. *42*, 2281–2297.

816 18. Eicher, A.K., Kechele, D.O., Sundaram, N., Zorn, A.M., Helmrath, M.A., Wells, J.M., Eicher, A.K.,
817 Kechele, D.O., Sundaram, N., Berns, H.M., et al. (2022). Functional human gastrointestinal
818 organoids can be engineered from three primary germ layers derived separately from pluripotent
819 stem cells. Cell Stem Cell *29*, 1–16.
820 19. El-Zaatari, M., Saqui-Salces, M., Waghray, M., Todisco, A., and Merchant, J.L. (2009). Sonic
821 hedgehog in gastric physiology and neoplastic transformation: Friend or foe? Curr. Opin.
822 Endocrinol. Diabetes Obes. *16*, 60–65.
823 20. Escaffit, F., Boudreau, F., and Beaulieu, J.F. (2005). Differential expression of claudin-2 along the
824 human intestine: Implication of GATA-4 in the maintenance of claudin-2 in differentiating cells. J.
825 Cell. Physiol. *203*, 15–26.
826 21. Fazilaty, H., Brügger, M.D., Valenta, T., Szczerba, B.M., Berkova, L., Doumpas, N., Hausmann, G.,
827 Scharl, M., and Basler, K. (2021). Tracing colonic embryonic transcriptional profiles and their
828 reactivation upon intestinal damage. Cell Rep. *36*.
829 22. Finak, G., McDavid, A., Yajima, M., Deng, J., Gersuk, V., Shalek, A.K., Slichter, C.K., Miller, H.W.,
830 McElrath, M.J., Prlic, M., et al. (2015). MAST: A flexible statistical framework for assessing
831 transcriptional changes and characterizing heterogeneity in single-cell RNA sequencing data.
832 Genome Biol. *16*, 1–13.
833 23. Fock, V., Plessl, K., Draxler, P., Otti, G.R., Fiala, C., Knöfler, M., and Pollheimer, J. (2015).
834 Neuregulin-1-mediated ErbB2-ErbB3 signalling protects human trophoblasts against apoptosis to
835 preserve differentiation. J. Cell Sci. *128*, 4306–4316.
836 24. Gore, Y., Starlets, D., Maharshak, N., Becker-Herman, S., Kaneyuki, U., Leng, L., Bucala, R., and
837 Shachar, I. (2008). Macrophage migration inhibitory factor induces B cell survival by activation of a
838 CD74-CD44 receptor complex. J. Biol. Chem. *283*, 2784–2792.

839 25. Gracz, A.D., Samsa, L.A., Fordham, M.J., Trotier, D.C., Zwarycz, B., Lo, Y.H., Bao, K., Starmer, J.,
840 Raab, J.R., Shroyer, N.F., et al. (2018). Sox4 Promotes Atoh1-Independent Intestinal Secretory
841 Differentiation Toward Tuft and Enteroendocrine Fates. Gastroenterology *155*, 1508-1523.e10.
842 26. Graham, R.P., Nair, A.A., Davila, J.I., Jin, L., Jen, J., Sukov, W.R., Wu, T.T., Appelman, H.D.,
843 Torres-Mora, J., Perry, K.D., et al. (2017). Gastroblastoma harbors a recurrent somatic MALAT1-
844 GLI1 fusion gene. Mod. Pathol. *30*, 1443–1452.
845 27. Gregorieff, A., Pinto, D., Begthel, H., Destrée, O., Kielman, M., and Clevers, H. (2005). Expression
846 Pattern of Wnt Signaling Components in the Adult Intestine. Gastroenterology *129*, 626–638.
847 28. Gulati, G.S., Sikandar, S.S., Wesche, D.J., Manjunath, A., Bharadwaj, A., Berger, M.J., Ilagan, F.,
848 Kuo, A.H., Hsieh, R.W., Cai, S., et al. (2020). Single-cell transcriptional diversity is a hallmark of
849 developmental potential. Science. *367*, 405–411.
850 29. Gunawardene, A.R., Corfe, B.M., and Staton, C.A. (2011). Classification and functions of
851 enteroendocrine cells of the lower gastrointestinal tract. Int. J. Exp. Pathol. *92*, 219–231.
852 30. Guo, W., and Frenette, P.S. (2014). Alternative CD44 splicing in intestinal stem cells and
853 tumorigenesis. Oncogene *33*, 537–538.
854 31. Guo, C., Chu, H., Gong, Z., Zhang, B., Li, C., Chen, J., and Huang, L. (2021). HOXB13 promotes
855 gastric cancer cell migration and invasion via IGF-1R upregulation and subsequent activation of
856 PI3K/AKT/mTOR signaling pathway. Life Sci. *278*, 119522.
857 32. Haghverdi, L., Lun, A.T.L., Morgan, M.D., and Marioni, J.C. (2018). Batch effects in single-cell RNA-
858 sequencing data are corrected by matching mutual nearest neighbors. Nat. Biotechnol. *36*, 421–
859 427.
860 33. Han, S., Fink, J., Jörg, D.J., Lee, E., Yum, M.K., Chatzeli, L., Merker, S.R., Josserand, M.,
861 Trendafilova, T., Andersson-Rolf, A., et al. (2019). Defining the Identity and Dynamics of Adult
862 Gastric Isthmus Stem Cells. Cell Stem Cell *25*, 342-356.e7.

863 34. Hao, Y., Hao, S., Andersen-Nissen, E., Mauck, W.M., Zheng, S., Butler, A., Lee, M.J., Wilk, A.J.,
864 Darby, C., Zager, M., et al. (2021). Integrated analysis of multimodal single-cell data. Cell *184*,
865 3573-3587.e29.
866 35. He, S., Wang, L.H., Liu, Y., Li, Y.Q., Chen, H.T., Xu, J.H., Peng, W., Lin, G.W., Wei, P.P., Li, B., et
867 al. (2020). Single-cell transcriptome profiling of an adult human cell atlas of 15 major organs.
868 Genome Biol. *21*, 1–34.
869 36. Higuchi, Y., Kojima, M., Ishii, G., Aoyagi, K., Sasaki, H., and Ochiai, A. (2015). Gastrointestinal
870 fibroblasts have specialized, diverse transcriptional phenotypes: A comprehensive gene expression
871 analysis of human fibroblasts. PLoS One *10*, 1–19.
872 37. Hosoi, K. (2016). Physiological role of aquaporin 5 in salivary glands. Pflugers Arch. Eur. J. Physiol.
873 *468*, 519–539.
874 38. Huang, N., Pérez, P., Kato, T., Mikami, Y., Okuda, K., Gilmore, R.C., Conde, C.D., Gasmi, B., Stein,
875 S., Beach, M., et al. (2021). SARS-CoV-2 infection of the oral cavity and saliva. Nat. Med. *27*, 892–
876 903.
877 39. Huggins, I.J., Bos, T., Gaylord, O., Jessen, C., Lonquich, B., Puranen, A., Richter, J., Rossdam, C.,
878 Brafman, D., Gaasterland, T., et al. (2017). The WNT target SP5 negatively regulates WNT
879 transcriptional programs in human pluripotent stem cells. Nat. Commun. *8*.
880 40. Jang, B.G., Lee, B.L., and Kim, W.H. (2013). Distribution of LGR5+ cells and associated
881 implications during the early stage of gastric tumorigenesis. PLoS One *8*.
882 41. Jang, B.G., Lee, B.L., and Kim, W.H. (2015). Intestinal stem cell markers in the intestinal metaplasia
883 of stomach and Barrett's esophagus. PLoS One *10*, 1–13.
884 42. Jang, J.W., Song, Y., Kim, S.H., Kim, J., and Seo, H.R. (2017). Potential mechanisms of CD133 in
885 cancer stem cells. Life Sci. *184*, 25–29.
886 43. Jardé, T., Chan, W.H., Rossello, F.J., Kaur Kahlon, T., Theocharous, M., Kurian Arackal, T., Flores,
887 T., Giraud, M., Richards, E., Chan, E., et al. (2020). Mesenchymal Niche-Derived Neuregulin-1

888 Drives Intestinal Stem Cell Proliferation and Regeneration of Damaged Epithelium. Cell Stem Cell
889 *27*, 646-662.e7.
890 44. Jin, S., Guerrero-Juarez, C.F., Zhang, L., Chang, I., Ramos, R., Kuan, C.H., Myung, P., Plikus, M.
891 V., and Nie, Q. (2021). Inference and analysis of cell-cell communication using CellChat. Nat.
892 Commun. *12*, 1–20.
893 45. Kaestner, K.H. (2019). The Intestinal Stem Cell Niche: A Central Role for Foxl1-Expressing
894 Subepithelial Telocytes. Cmgh *8*, 111–117.
895 46. Kania, A., and Klein, R. (2016). Mechanisms of ephrin-Eph signalling in development, physiology
896 and disease. Nat. Rev. Mol. Cell Biol. *17*, 240–256.
897 47. Katoh, Y., and Katoh, M. (2006). Hedgehog signaling pathway and gastrointestinal stem cell
898 signaling network (Review). Int. J. Mol. Med. *18*, 1019–1023.
899 48. Kim, T.H., and Shivdasani, R.A. (2016). Stomach development, stem cells and disease. Dev. *143*,
900 554–565.
901 49. Kim, B.M., Buchner, G., Miletich, I., Sharpe, P.T., and Shivdasani, R.A. (2005). The stomach
902 mesenchymal transcription factor barx1 specifies gastric epithelial identity through inhibition of
903 transient Wnt signaling. Dev. Cell *8*, 611–622.
904 50. Koch, S. (2017). Extrinsic control of Wnt signaling in the intestine. Differentiation *97*, 1–8.
905 51. Korsunsky, I., Millard, N., Fan, J., Slowikowski, K., Zhang, F., Wei, K., Baglaenko, Y., Brenner, M.,
906 Loh, P. ru, and Raychaudhuri, S. (2019). Fast, sensitive and accurate integration of single-cell data
907 with Harmony. Nat. Methods *16*, 1289–1296.
908 52. Kosaki, K., Bassi, M.T., Kosaki, R., Lewin, M., Belmont, J., Schauer, G., and Casey, B. (1999).
909 Characterization and Mutation Analysis of Human LEFTY A and LEFTY B , Homologues of Murine
910 Genes Implicated in Left-Right Axis Development. Am. J. Hum. Genet. *64*, 712–721.
911 53. Ma, X., Stelnicki, E., Rozenfeld, S., Oda, Y., and Largman, C. (2003). HOXB13 Homeodomain
912 Protein is Cytoplasmic Throughout Fetal Skin Development. Dev. Dyn. *227*, 192–202.

913 54. Mao, W., Chen, J., Peng, T.L., Yin, X.F., Chen, L.Z., and Chen, M.H. (2012). Downregulation of
914 gastrokine-1 in gastric cancer tissues and restoration of its expression induced gastric cancer cells
915 to apoptosis. J. Exp. Clin. Cancer Res. *31*, 1–10.
916 55. Matsumoto, M., Yokoyama, H., Suzuki, H., Shiraishi-Yokoyama, H., and Hibi, T. (2005). Retinoic
917 acid formation from retinol in the human gastric mucosa: Role of class IV alcohol dehydrogenase
918 and its relevance to morphological changes. Am. J. Physiol. - Gastrointest. Liver Physiol. *289*, 429–
919 433.
920 56. Meno, C., Shimono, A., Saijoh, Y., Yashiro, K., Mochida, K., Ohishi, S., Noji, S., Kondoh, H., and
921 Hamada, H. (1998). Lefty-1 Is Required for Left-Right Determination As a Regulator of Lefty-2 and
922 Nodal. Cell *94*, 287–297.
923 57. Meyer, D., and Birchmeier, C. (1995). Multiple essential functions of neuregulin in development.
924 Nature *14*, 386–390.
925 58. Miyoshi, H., Ajima, R., Luo, T, C., Yamaguchi, P, T., and Stappenbeck, S, T. (2012). Wnt5a
926 Potentiates TGF- b Signaling - First LWNR conditioned media. Science. *338*, 108–113.
927 59. Morgan, R., and Pandha, H.S. (2017). HOX transcription factors and the prostate tumor
928 microenvironment. J. Cancer Metastasis Treat. *3*, 278.
929 60. Nam, K.T., Lee, H., Sousa, J.F., Weis, V.G., O'Neal, R.L., Finke, P.E., Romerogallo, J., Shi, G.,
930 Mills, J.C., Peek, R.M., et al. (2010). Mature chief cells are cryptic progenitors for metaplasia in the
931 stomach. Gastroenterology *139*, 2028-2037.e9.
932 61. Nestorowa, S., Hamey, F.K., Pijuan Sala, B., Diamanti, E., Shepherd, M., Laurenti, E., Wilson, N.K.,
933 Kent, D.G., and Göttgens, B. (2016). A single-cell resolution map of mouse hematopoietic stem and
934 progenitor cell differentiation. Blood *128*, e20–e31.
935 62. Nie, S., and Yuan, Y. (2020). The Role of Gastric Mucosal Immunity in Gastric Diseases. J.
936 Immunol. Res. *2020*.

937 63. Ormestad, M., Astorga, J., Landgren, H., Wang, T., Johansson, B.R., Miura, N., and Carlsson, P.
938 (2006). Foxf1 and Foxf2 control murine gut development by limiting mesenchymal Wnt signaling
939 and promoting extracellular matrix production. Development *133*, 833–843.
940 64. Owen, R.P., White, M.J., Severson, D.T., Braden, B., Bailey, A., Goldin, R., Wang, L.M., Ruiz-Puig,
941 C., Maynard, N.D., Green, A., et al. (2018). Single cell RNA-seq reveals profound transcriptional
942 similarity between Barrett's oesophagus and oesophageal submucosal glands. Nat. Commun. *9*.
943 65. Pitulescu, M.E., and Adams, R.H. (2010). Eph/ephrin molecules - A hub for signaling and
944 endocytosis. Genes Dev. *24*, 2480–2492.
945 66. Radyk, M.D., Burclaff, J., Willet, S.G., and Mills, J.C. (2018). Metaplastic Cells in the Stomach Arise,
946 Independently of Stem Cells, via Dedifferentiation or Transdifferentiation of Chief Cells.
947 Gastroenterology *154*, 839-843.e2.
948 67. Ramalho-santos, M., Melton, D.A., and Mcmahon, A.P. (2000). Hedgehog signals regulate multiple
949 aspects of gastrointestinal development. Development *127*, 2763–2772.
950 68. Romi, B., Soldaini, E., Pancotto, L., Castellino, F., del Giudice, G., and Schiavetti, F. (2011).
951 Helicobacter pylori induces activation of human peripheral γδ+ T lymphocytes. PLoS One *6*.
952 69. Roy, S.A.B., Allaire, J.M., Ouellet, C., Maloum-Rami, F., Pomerleau, V., Lemieux, É., Babeu, J.P.,
953 Rousseau, J., Paquet, M., Garde-Granger, P., et al. (2016). Loss of mesenchymal bone
954 morphogenetic protein signaling leads to development of reactive stroma and initiation of the gastric
955 neoplastic cascade. Sci. Rep. *6*, 1–15.
956 70. Van de Sande, B., Flerin, C., Davie, K., De Waegeneer, M., Hulselmans, G., Aibar, S., Seurinck, R.,
957 Saelens, W., Cannoodt, R., Rouchon, Q., et al. (2020). A scalable SCENIC workflow for single-cell
958 gene regulatory network analysis. Nat. Protoc. *15*, 2247–2276.
959 71. Sathe, A., Grimes, S.M., Lau, B.T., Chen, J., Suarez, C., Huang, R.J., Poultsides, G., and Ji, H.P.
960 (2020). Single-Cell Genomic Characterization Reveals the Cellular Reprogramming of the Gastric
961 Tumor Microenvironment. Clin. Cancer Res. *26*, 2640–2653.

962 72. Shi, X., Leng, L., Wang, T., Wang, W., Du, X., Li, J., McDonald, C., Chen, Z., Murphy, J.W., Lolis,
963 E., et al. (2006). CD44 Is the Signaling Component of the Macrophage Migration Inhibitory Factor-
964 CD74 Receptor Complex. Immunity *25*, 595–606.
965 73. Shinohara, M., Mao, M., Keeley, T.M., Elzaatari, M., Lee, H., Eaton, K.A., Samuelson, L.C.,
966 Merchant, J.L., Goldenring, J.R., and Todisco, A. (2010). Bone morphogenetic protein signaling
967 regulates gastric epithelial cell development and proliferation in mice. Gastroenterology *139*, 2050-
968 2060.e2.
969 74. Shyh-Chang, N., and Ng, H.H. (2017). The metabolic programming of stem cells. Genes Dev. *31*,
970 336–346.
971 75. Sidney, L.E., Branch, M.J., Dunphy, S.E., Dua, H.S., and Hopkinson, A. (2014). Concise review:
972 evidence for CD34 as a common marker for diverse progenitors. Stem Cells *32*, 1380–1389.
973 76. Simmini, S., Bialecka, M., Huch, M., Kester, L., Van De Wetering, M., Sato, T., Beck, F., Van
974 Oudenaarden, A., Clevers, H., and Deschamps, J. (2014). Transformation of intestinal stem cells
975 into gastric stem cells on loss of transcription factor Cdx2. Nat. Commun. *5*, 1–10.
976 77. Spit, M., Koo, B.K., and Maurice, M.M. (2018). Tales from the crypt: Intestinal niche signals in tissue
977 renewal, plasticity and cancer. Open Biol. *8*.
978 78. Stuart, T., Butler, A., Hoffman, P., Hafemeister, C., Papalexi, E., Mauck, W.M., Hao, Y., Stoeckius,
979 M., Smibert, P., and Satija, R. (2019). Comprehensive Integration of Single-Cell Data. Cell *177*,
980 1888-1902.e21.
981 79. Tabibzadeh, S., and Hemmati-Brivanlou, A. (2006). Lefty at the Crossroads of “Stemness” and
982 Differentiative Events . Stem Cells *24*, 1998–2006.
983 80. Tan, S.H., Swathi, Y., Tan, S., Goh, J., Seishima, R., Murakami, K., Oshima, M., Tsuji, T., Phuah,
984 P., Tan, L.T., et al. (2020). AQP5 enriches for stem cells and cancer origins in the distal stomach.
985 Nature *578*, 437–443.

986 81. The Tabula Sapiens Consortium (2022). The Tabula Sapiens: A multiple-organ, single-cell
987 transcriptomic atlas of humans. Science. *376*.
988 82. Thompson, C.A., DeLaForest, A., and Battle, M.A. (2018). Patterning the gastrointestinal epithelium
989 to confer regional-specific functions. Dev. Biol. *435*, 97–108.
990 83. Tischler, J., Gruhn, W.H., Reid, J., Allgeyer, E., Buettner, F., Marr, C., Theis, F., Simons, B.D.,
991 Wernisch, L., and Surani, M.A. (2019). Metabolic regulation of pluripotency and germ cell fate
992 through α-ketoglutarate. EMBO J. *38*, 1–15.
993 84. Voutilainen, M., Juhola, M., Pitkänen, R., Färkkilä, M., and Sipponen, P. (2002).
994 Immunohistochemical study of neuroendocrine cells at the gastric cardia mucosa. J. Clin. Pathol.
995 *55*, 767–769.
996 85. Westerlund, M., Belin, A.C., Felder, M.R., Olson, L., and Galter, D. (2007). High and complementary
997 expression patterns of alcohol and aldehyde dehydrogenases in the gastrointestinal tract:
998 Implications for Parkinson's disease. FEBS J. *274*, 1212–1223.
999 86. Wölffling, S., Daddi, A.A., Imai-Matsushima, A., Fritsche, K., Goosmann, C., Traulsen, J., Lisle, R.,
1000 Schmid, M., Reines-Benassar, M. del M., Pfannkuch, L., et al. (2021). EGF and BMPs Govern
1001 Differentiation and Patterning in Human Gastric Glands. Gastroenterology *161*, 623-636.e16.
1002 87. Wroblewski, L.E., Peek, R.M., and Wilson, K.T. (2010). Helicobacter pylori and gastric cancer:
1003 Factors that modulate disease risk. Clin. Microbiol. Rev. *23*, 713–739.
1004 88. Wuputra, K., Ku, C.C., Kato, K., Wu, D.C., Saito, S., and Yokoyama, K.K. (2021). Translational
1005 models of 3-D organoids and cancer stem cells in gastric cancer research. Stem Cell Res. Ther. *12*,
1006 1–16.
1007 89. Xie, B., Bai, B., Xu, Y., Liu, Y., Lv, Y., Gao, X., Wu, F., Fang, Z., Lou, Y., Pan, H., et al. (2019).
1008 Tumor-suppressive function and mechanism of HOXB13 in right-sided colon cancer. Signal
1009 Transduct. Target. Ther. *4*.

1010 90. Ye, W., Takabayashi, H., Yang, Y., Mao, M., Hibdon, E.S., Samuelson, L.C., Eaton, K.A., and
1011 Todisco, A. (2018). Regulation of Gastric Lgr5+ve Cell Homeostasis by Bone Morphogenetic
1012 Protein (BMP) Signaling and Inflammatory Stimuli. Cmgh *5*, 523–538.
1013 91. Yoon, J.H., Choi, W.S., Kim, O., Choi, S.S., Lee, E.K., Nam, S.W., Lee, J.Y., and Park, W.S. (2015).
1014 NKX6.3 controls gastric differentiation and tumorigenesis. Oncotarget *6*, 28425–28439.
1015 92. Yoon, J.H., Choi, S.S., Kim, O., Choi, W.S., Park, Y.K., Nam, S.W., Lee, J.Y., and Park, W.S.
1016 (2016). Inactivation of NKX6.3 in the stomach leads to abnormal expression of CDX2 and SOX2
1017 required for gastric-to-intestinal transdifferentiation. Mod. Pathol. *29*, 194–208.
1018 93. Young, M.D., and Behjati, S. (2020). SoupX removes ambient RNA contamination from droplet-
1019 based single-cell RNA sequencing data. Gigascience *9*, 1–10.
1020 94. Yu, M., Zhan, J., and Zhang, H. (2020). HOX family transcription factors: Related signaling
1021 pathways and post-translational modifications in cancer. Cell. Signal. *66*, 109469.
1022 95. Zabala, M., Lobo, N.A., Antony, J., Heitink, L.S., Gulati, G.S., Lam, J., Parashurama, N., Sanchez,
1023 K., Adorno, M., Sikandar, S.S., et al. (2020). LEFTY1 Is a Dual-SMAD Inhibitor that Promotes
1024 Mammary Progenitor Growth and Tumorigenesis. Cell Stem Cell *27*, 284-299.e8.
1025 96. Zhang, M., Liu, Y., and Chen, Y.G. (2020). Generation of 3D human gastrointestinal organoids:
1026 principle and applications. Cell Regen. *9*, 1–13.
1027 97. Zhang, P., Yang, M., Zhang, Y., Xiao, S., Lai, X., Tan, A., Du, S., and Li, S. (2019). Dissecting the
1028 Single-Cell Transcriptome Network Underlying Gastric Premalignant Lesions and Early Gastric
1029 Cancer. Cell Rep. *27*, 1934-1947.e5.
1030 98. Zimmerman, L.B., Jesu, M. De, and Harland, R.M. (1996). The Spemann Organizer Signal noggin
1031 Binds and Inactivates Bone Morphogenetic Protein 4. *86*, 599–606.
1032

1033 **STAR*METHODS**

1034 **KEY RESOURCES TABLE**

REAGENT or RESOURCE	SOURCE	IDENTIFIER
Antibodies		
Anti-GKN1 antibody	Merck	Cat# HPA047684, RRID: AB_2680120
Anti-ADH1C antibody	Abcam	ab238486
Anti-ACKR1 antibody	Merck	Cat# HPA016421, RRID: AB_1849219
Anti-PLVAP antibody	Merck	Cat# HPA002279, RRID: AB_1079636
CD31 antibody	Dako	Cat# M0823, RRID: AB_2114471
LEFTY1 rabbit mAb antibody	Cell Signaling Technology	Cat# 12647, RRID: AB_2797977
Anti-CD44 antibody	Abcam	Cat# ab16728, RRID: AB_443447
Anti-ephrin B2 antibody	Abcam	Cat# ab131536, RRID: AB_11156896
Human/mouse EPHB2 polyclonal antibody	R&D systems	Cat# AF467, RRID: AB_355375
Anti-NKX6-3	Merck	Cat# HPA042790, RRID: AB_10796678
Anti-HOXB13 antibody	Abcam	Cat# ab201682
Beta-tubulin antibody	Abcam	Cat# ab52623, RRID: AB_869991
Biological Samples		
Human gastric specimen	This study	Table S1
Critical Commercial Assays		
RNAScope Duplex	ACD	Cat# 322430
Chromium Controller and the	10X Genomics	

Single-Cell Reagent Kit 3' v2		
Deposited Data		
Raw and analyzed data	This study	
Stanford	(Sathe et al., 2020)	dbGAP: phs001818.v1.p1
Tsinghua	(Zhang et al., 2019)	GSE134520
Recombinant DNA		
hs-LEFTY1-C2	ACD	Cat No. 415651-C2
hs-LGR5	ACD	Cat No. 311021
hs-HHIP-C2	ACD	Cat No. 464811-C2
hs-SFRP1-C2	ACD	Cat No. 429381-C2
hs-WNT5A	ACD	Cat No. 604921
hs-NOG-C2	ACD	Cat No. 416521-C2
hs-BMP4	ACD	Cat No. 454301
hs-SP5	ACD	Cat No. 406541
Software and Algorithms		
Cell Ranger	10X Genomics	
Seurat 3.1.5	(Stuart et al., 2019) (Hao et al., 2021)	https://satijalab.org/seurat/index.html
Harmony 1.0	(Korsunsky et al., 2019)	https://portals.broadinstitute.org/harmony/index.html
SingleR 1.0.6	(Aran et al., 2019)	https://bioconductor.org/packages/devel/bioc/vignettes/SingleR/inst/doc/SingleR.html
scds 1.1.2	(Bais and Kostka, 2020)	https://bioconductor.org/packages/devel/bioc/vignettes/scds/inst/doc/scds.html
CytoTRACE 0.3.3	(Gulati et al., 2020)	https://cytotrace.stanford.edu/
monocle3 1.0.0	(Cao et al., 2019)	https://cole-trapnell-lab.github.io/monocle3/
pySCENIC 0.11.2	(Aibar et al., 2017) (Van de Sande et al., 2020)	https://scenic.aertslab.org/
cellchat 1.1.0	(Jin et al., 2021)	http://www.cellchat.org/

1035

1036 **RESOURCE AVAILABILITY**

1037 **Lead contact**

1038 Further information and requests for resources should be directed to and will be fulfilled by the lead

1039 contact, Shumpei Ishikawa (ishum-prm@m.u-tokyo.ac.jp).

1040 **EXPERIMENTAL MODELS AND SUBJECT DETAILS**

1041 **Materials and methods**

1042 **Human specimens**

1043 This study was approved by the Institutional Review Board of The University of Tokyo and written

1044 informed consent was obtained from patients. The stomach tissues analyzed in this study were obtained

1045 from 15 patients who underwent gastrectomy at The University of Tokyo Hospital from 2017 to 2019.

1046 Fresh specimens of noncancerous stomach tissues were obtained immediately after surgeries and

1047 subjected to scRNA-seq. Fresh frozen specimens and formalin-fixed and paraffin-embedded (FFPE)

1048 specimens of the same patients were also preserved for histopathological examination.

1049

1050 **Single-cell RNA sequencing**

1051 For cases #3–12 and #14–18 listed in Table S1, freshly obtained 3–5-mm-sized specimens from normal

1052 stomach tissues were immediately subjected to scRNA-seq. Specimens were cut into pieces of ~1 mm

1053 in size and incubated in collagenase/hyaluronidase (STEMCELL Technologies, Canada) diluted with

1054 Dulbecco's modified Eagle medium [FUJIFILM Wako Pure Chemical Corporation (FUJIFILM), Japan] at

1055 37°C for 30 min with mild agitation, according to the manufacturer's protocol. Single-cell fractions in the

1056 incubated specimens were separated using a 40-μm Cell Strainer (CORNING, USA) with additional

1057 filtration conducted using phosphate-buffered saline (PBS; FUJIFILM). The number of cells obtained in

1058 single-cell fractions was counted using a hemocytometer (BMS, Japan) following the manufacturer's

1059 protocol. In total, 10,000 cells were subjected to analysis in a Chromium Controller (10X Genomics,

1060 USA) following the manufacturer's instructions. A scRNA-seq library was constructed using Chromium

1061 Single-Cell 3′ Reagent Kits ver 2 (10X Genomics), after which the quantification and qualification of
1062 sequencing libraries was performed using an Agilent Bioanalyzer (Agilent Technologies, USA) with a
1063 High-Sensitivity DNA Kit LabChip (Agilent Technologies).

1064 For cases #7–12 and #14–18, we purified B cell populations used for another experimental
1065 purpose (not analyzed in the present study) from the residual cell fractions of the above-mentioned
1066 scRNA-seq experiments. B cell fractions were purified using an EasySep Human CD19 Positive
1067 Selection Kit II (STEMCELL Technologies) according to the manufacturer's protocol, after which the cells
1068 were resuspended in PBS (FUJIFILM). The purity of the magnet bead-based cellular purifications was
1069 considered relatively low; thus, it was considered that a substantial number of mixed cellular populations
1070 other than B cells were still included in these samples. Therefore, we included the scRNA-seq data of
1071 these B cell-purified samples in combination with the above-mentioned scRNA-seq only when the
1072 enriched B cell populations did not affect the purposes and results of our data analyses. Thereafter,
1073 10,000 cells were subjected to scRNA-seq using the Chromium Controller (10X Genomics) following the
1074 manufacturer's instructions. A scRNA-seq library was constructed using Chromium Single-Cell V(D)J
1075 Reagent Kits (10X Genomics) combined with Chromium Single-Cell 5′ Library & Gel Bead Kits (10X
1076 Genomics), after which the sequencing libraries were quantified and qualified using an Agilent
1077 Bioanalyzer (Agilent Technologies) with a High-Sensitivity DNA Kit LabChip (Agilent Technologies).

1078 The entire scRNA-seq library was subjected to next-generation sequencing using an Illumina
1079 NovaSeq platform (Illumina, USA). This sequencing was conducted by iLAC (Ibaraki, Japan).

1080

1081 **Data preprocessing for scRNA-seq**

1082 Sequencing data were aligned to human genome GRCh38, and the unique molecular identifiers for
1083 each cell were counted using Cell Ranger version 3.1 (10X Genomics). Ambient RNA removal was
1084 performed with SoupX version 1.3.7 (Young and Behjati, 2020) using hemoglobin genes and
1085 immunoglobulin genes to estimate contamination fractions. Gene expression matrices of Stanford

University and Tsinghua University were downloaded from https://www.ncbi.nlm.nih.gov/projects/gap/cgi-bin/study.cgi?study_id=phs001818.v1.p1 and https://www.ncbi.nlm.nih.gov/geo/query/acc.cgi?acc=GSE134520, respectively. All data were then merged using Seurat R package version 3.1.5 (Stuart et al., 2019), and the batch effects among the samples were removed using Harmony R package version 1.0 (Korsunsky et al., 2019). Cells with low quality were then filtered out based on the proportion of mitochondrial gene counts. We used a cell-type specific cutoff value based on the following procedure. First, we inferred the cell types using SingleR version 1.0.6 (Aran et al., 2019) and reference transcriptomic datasets. We then removed cells with >25% mitochondrial genes in the epithelial cell lineage and >15% mitochondrial genes in other cells. Finally, we used scds R package version 1.1.2 (Bais and Kostka, 2020) for doublet cell detection.

We applied the “LogNormalize” function that normalized the gene expression of each cell according to the total expression, multiplied this by a scale factor 10,000, and log-transformed the result using the NormalizeData() function in Seurat.

Clustering, visualization, and cell annotation

Principal components were calculated based on the normalized gene expression profiles. The number of principal components was determined using a Jackstraw plot, the p-value thresholds of which were 0.05. tSNE and UMAP dimensionality reduction was performed using the Seurat functions “RunTSNE” and “RunUMAP,” respectively. Cell clusters were identified using the “FindClusters” function in Seurat. Differentially expressed genes were obtained using the “FindAllMarkers” function via MAST (Finak et al., 2015) with the number of genes detected in each cell used as a latent variable. The cell cycle phases for each cell were estimated based on the gene expression of cell cycle marker genes (Nestorowa et al., 2016).

Annotation of IM status

In our dataset, IM status was determined based on histology by experienced pathologists. For the Tsinghua University dataset, because IM status was already annotated by the authors, we used the existing annotations. For the Stanford University dataset, we calculated the percentage of intestinal cells in all epithelial cells for each sample, and the IM status was estimated by comparing this percentage with those of the Tsinghua University dataset and our own dataset.

Transcriptional entropy and trajectory analysis

Using the count data of scRNA-seq and cell-type annotations from Seurat as input, CytoTRACE (Gulati et al., 2020) analysis was conducted to calculate transcriptional entropy. Trajectory analysis was performed using monocle3 (Cao et al., 2019) with the same input as that used in CytoTRACE. In monocle3, batch effect removal was conducted using a function implemented in the software (Haghverdi et al., 2018).

Gene regulatory network and cell–cell communication analysis

The gene regulatory networks for epithelial and fibroblast cells were inferred using the SCENIC and pySCENIC pipelines (Aibar et al., 2017; Van de Sande et al., 2020). To confirm reproducibility, gene regulatory network analysis was performed 10 times. The Seurat object with cell-type annotation data was converted to a loom object using the loomR library to generate input data for SCENIC. CCC analysis was conducted using Cellchat (Jin et al., 2021) with count data and cell-type annotations used as input data.

Hematoxylin and eosin staining

Fresh frozen and FFPE specimens were sliced to thicknesses of 4 μm and subjected to hematoxylin and eosin (H&E) staining. Histopathological slides of fresh frozen specimens were snap-fixed with 4% paraformaldehyde phosphate buffer solution (FUJIFILM) for 10 min at room temperature, and the slides

1136 of FFPE specimens were deparaffinized and rehydrated via immersions in xylene (#241-00091;
1137 FUJIFILM) and ethanol (#057-00451; FUJIFILM), respectively. Hematoxylin (#6187-4P; Sakura Finetek
1138 Japan, Japan) and eosin (#8660; Sakura Finetek) solutions were then used to achieve H&E staining
1139 following the manufacturer's protocols. The stained slides were dehydrated via immersions in ethanol
1140 and xylene, respectively, after which glass coverslips (Matsunami Glass, Japan) with Marinol
1141 (#4197193, Muto Pure Chemicals, Japan) were used to cover the stained slides. H&E-stained images
1142 were then captured using a Hamamatsu Nanozoomer 2.0 HT whole slide scanner (Hamamatsu
1143 Photonics K.K., Japan).
1144
1145 **Immunohistochemistry**
1146 For IHC, histopathological slides with FFPE specimens were deparaffinized and rehydrated via
1147 immersions in xylene (#241-00091; FUJIFILM) and ethanol (#057-00451; FUJIFILM), respectively. The
1148 slides were then autoclaved for 5 min at 120°C while immersed in citrate buffer (pH 6.0) (Abcam,
1149 Cambridge, UK). Endogenous peroxidase activity was consumed using 0.3% hydrogen peroxide (Sigma
1150 Aldrich, USA) in methanol (#137-01823; FUJIFILM) for 15 min, after which the slides were washed using
1151 distilled water. Nonspecific protein–protein reactions were blocked by incubating the slides in 2% bovine
1152 serum albumin (Sigma Aldrich, USA)/PBS (FUJIFILM) for 15 min at room temperature. The following
1153 primary antibodies were used, which were incubated on the slide at 4°C overnight: GKN1 (1:1,000;
1154 Merck, HPA047684), ADH1C (1:2,000; Abcam, ab238486), ACKR1 (1:200; Merck, HPA016421), PLVAP
1155 (1:100; Merck, HPA002279), CD31 (1:100; Dako, M0823), LEFTY1 (1:1,000; Cell Signaling Technology,
1156 #12647), CD44 (1:200; Abcam, ab157107), EFNB2 (1:200; Abcam, ab131536), EPHB2 (1:200; R&D
1157 systems, AF467), NKX6-3 (1:1,000; Merck, HPA042790), HOXB13 (1:3,000; Abcam, ab201682), and
1158 TUBB3 (1:200; Abcam, ab52623). After washing the slides with PBS (FUJIFILM) three times, Histostar
1159 (Ms+Rb) for Human Tissue (MBL, Japan) was used as a secondary antibody, and the slides were
1160 washed using PBS (FUJIFILM) three times. IHC signals were developed using Histostar DAB Substrate

1161 Solution (MBL) according to the manufacturer's protocol. Nuclear staining was performed using a
1162 hematoxylin (#6187-4P; Sakura Finetek Japan) solution. The stained slides were dehydrated using
1163 immersions in ethanol followed by xylene, after which glass coverslips (Matsunami Glass) with Marinol
1164 (#4197193; Muto Pure Chemicals) were used to cover the stained slides. IHC images were captured
1165 using a Hamamatsu Nanozoomer 2.0 HT whole slide scanner (Hamamatsu Photonics K.K., Japan).
1166

1167 **RNAScope**

1168 To achieve ISH, a RNAScope 2.5 HD Duplex Assay (Advanced Cell Diagnostics, Inc., Hayward, CA,
1169 USA) was performed according to the manufacturer's instructions. The method used to prepare FFPE
1170 samples was the same as that used for IHC analysis. A list of the probes used is provided in the key
1171 resources table.
1172

1173 **Signal magnification of RNAScope**

1174 We extracted green or red signals from the image of RNAScope and magnified these signals 100 times
1175 using python library cv2 and PIL. Green and red signal thresholds were defined manually.
1176

1177 **Table S1. Sample metadata.**

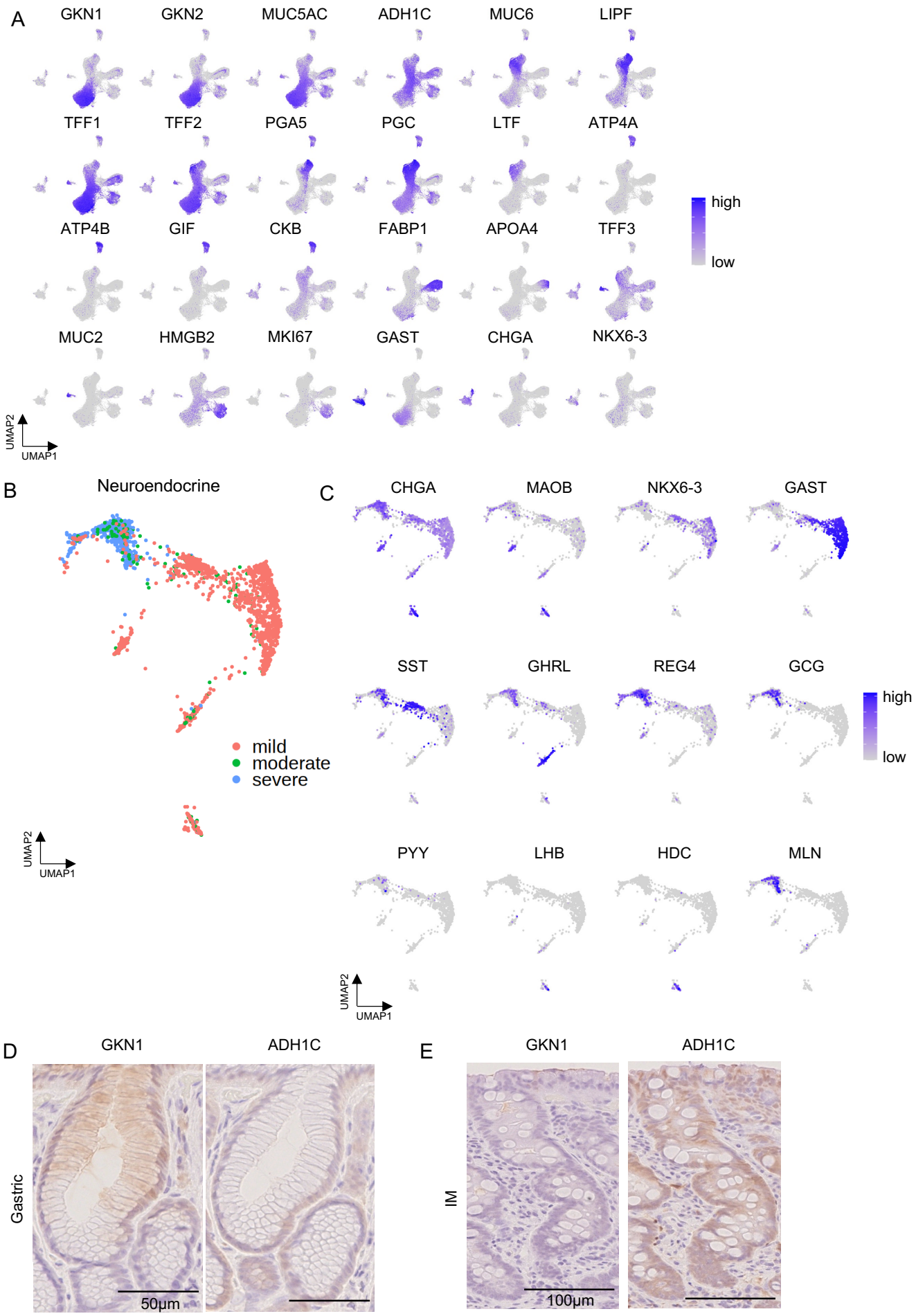
A
GKN1
GKN2
MUC5AC
ADH1C
MUC6
LIPF
TFF1
TFF2
PGA5
PGC
LTF
ATP4A
ATP4B
GIF
CKB
FABP1
APOA4
TFF3
MUC2
HMGB2
MKI67
GAST
CHGA
NKX6-3
high
low
UMAP2
UMAP1
B
Neuroendocrine
mild
moderate
severe
UMAP2
UMAP1
C
CHGA
MAOB
NKX6-3
GAST
SST
GHRL
REG4
GCG
PYY
LHB
HDC
MLN
high
low
UMAP2
UMAP1
D
GKN1
ADH1C
Gastric
50μm
E
GKN1
ADH1C
IM
100μm

1178

1179 **Figure S1. Marker genes of epithelial cells and neuroendocrine-specific cells (related to Figure**
1180 **1).**

1181 (A) Representative epithelial cell marker gene expression selected from differentially expressed
1182 genes.

1183 (B) UMAP of neuroendocrine cells with IM severeness. Almost all neuroendocrine cells from severe
1184 or moderate IM samples express REG4.

1185 (C) Several enzymes and marker genes of neuroendocrine cells. Almost all *GAST*+ cells are from
1186 mild IM samples, and *GCG* and *MLN*+ cells are from severe or moderate samples. Rare
1187 neuroendocrine cells such as *LHB*+ or *HDC*+ cells were identified.

1188 (D, E) IHC of GKN1 and ADH1C in the stomach and IM, respectively. GKN1 expression is limited in
1189 the superficial region in normal gastric mucosa. ADH1C expression is in the deeper region in
1190 normal gastric mucosa and in all IM region.

1191

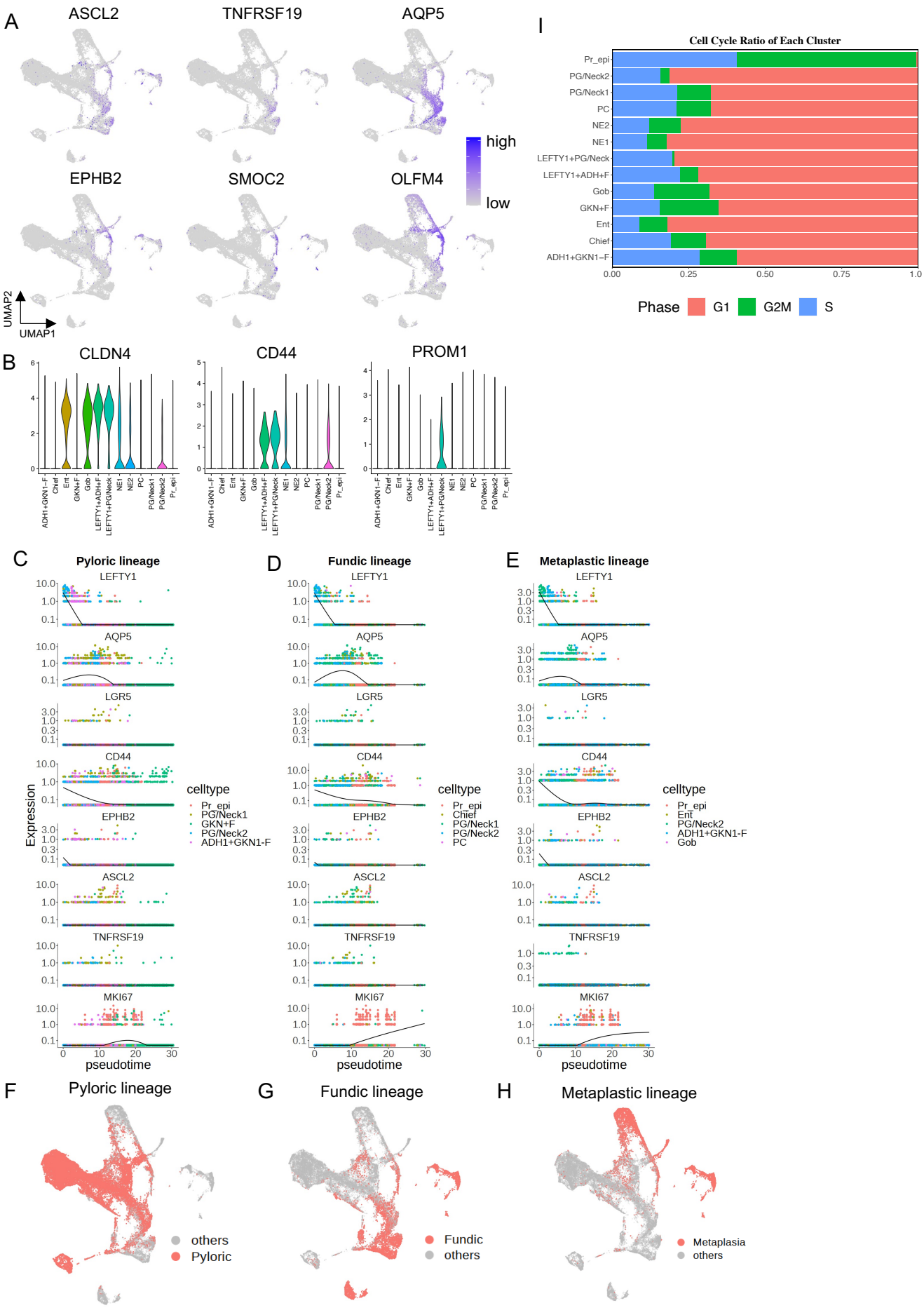
A
ASCL2
TNFRSF19
AQP5
EPHB2
SMOC2
OLFM4
high
low
UMAP2
UMAP1
I
Cell Cycle Ratio of Each Cluster
Pr_epi
PG/Neck2
PG/Neck1
PC
NE2
NE1
LEFTY1+PG/Neck
LEFTY1+ADH+F
Gob
GKN+F
Ent
Chief
ADH1+GKN1−F
0.00
0.25
0.50
0.75
1.0
Phase
G1
G2M
S
B
CLDN4
CD44
PROM1
C
Pyloric lineage
D
Fundic lineage
E
Metaplastic lineage
LEFTY1
AQP5
LGR5
CD44
EPHB2
ASCL2
TNFRSF19
MKI67
Expression
pseudotime
celltype
Pr_epi
PG/Neck1
GKN+F
PG/Neck2
ADH1+GKN1-F
Chief
PC
Ent
Gob
F
Pyloric lineage
G
Fundic lineage
H
Metaplastic lineage
others
Pyloric
Fundic
others
Metaplasia
others

1192

1193 **Figure S2. Gastrointestinal stemness-associated genes enriched in LEFTY1+ and pseudotime**

1194 **dynamics (related to Figure 2).**

1195 (A, B) Stem cell-associated gene expression in the epithelial cells. These marker genes are

1196 expressed in LEFTY1+ cells.

1197 (C–E) Pseudotime plots of representative stem cell markers in each lineage. LEFTY1 expression is

1198 highest in the earliest time in pseudotime among other stemness-associated genes. MKI67

1199 expression is high in the middle of the pseudotime.

1200 (F–H) UMAP showing each lineage cell; Pyloric lineages cell include GKN+F, ADH1+GKN1-F,

1201 PG/Neck1, PG/Neck2, and Pr_epi; Fundic lineage cells: PG/Neck1, PG/Neck2, PC, Chief,

1202 Pr_epi; Metaplastic lineage cells; PG/Neck2, ADH1+GKN1-F, Gob, Ent, Pr_epi.

1203 (I) Proportion of cell cycle phases in each cluster. Almost all proliferating epithelial cells show G2M or

1204 S phase. The G2M phase was detected less frequently in LEFTY1+ PG/Neck cells, which was

1205 compatible with being quiescent. See methods for cell cycle analysis details.

1206

1207

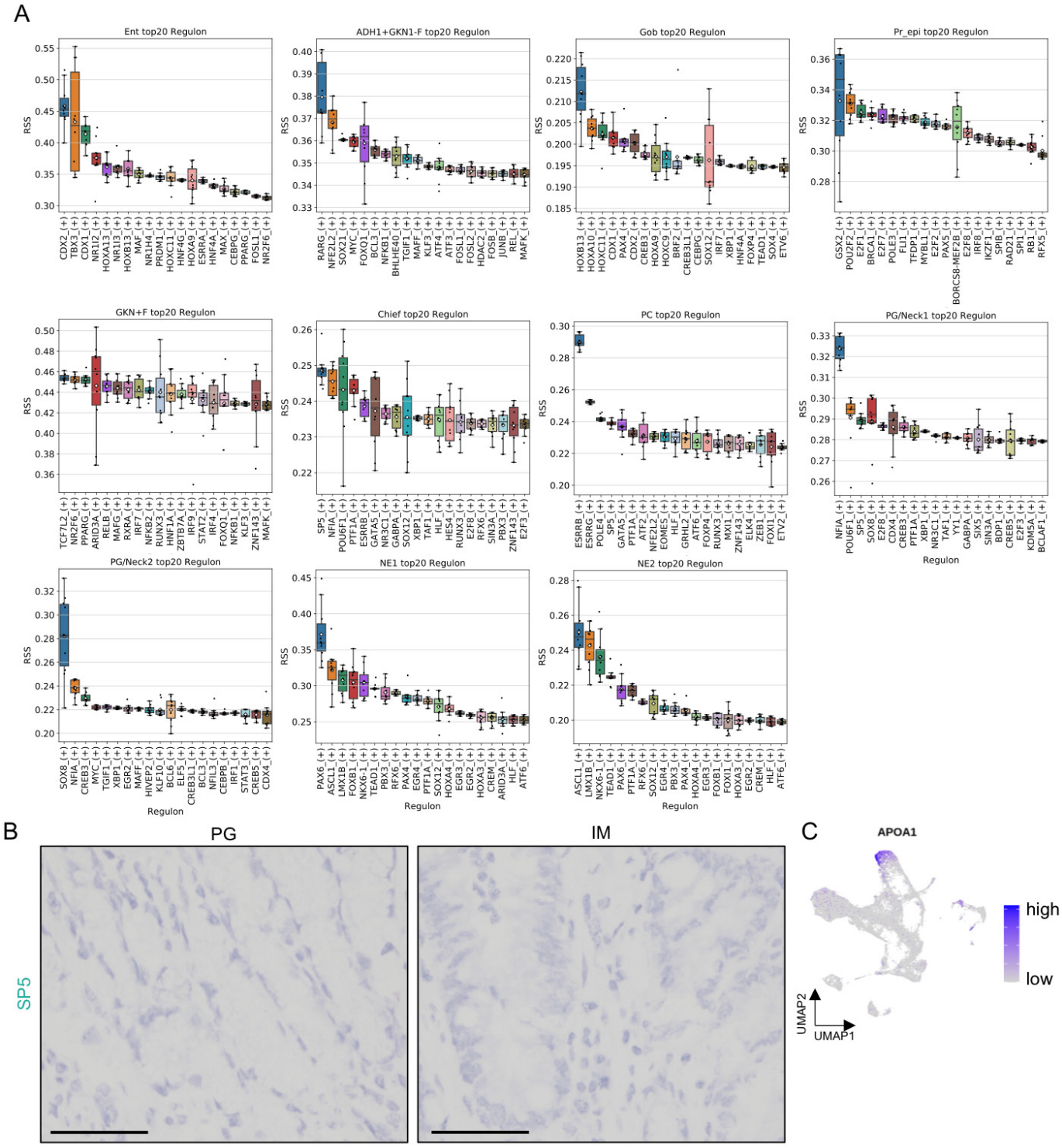
A
Ent top20 Regulon
ADH1+GKN1-F top20 Regulon
Gob top20 Regulon
Pr_epi top20 Regulon
GKN+F top20 Regulon
Chief top20 Regulon
PC top20 Regulon
PG/Neck1 top20 Regulon
PG/Neck2 top20 Regulon
NE1 top20 Regulon
NE2 top20 Regulon
RSS
Regulon
B
PG
IM
SP5
C
APOA1
high
low
UMAP2
UMAP1

1208

1209 **Figure S3. Top 20 regulons, except LEFTY1+ cell clusters, in the epithelial cells (related to Figure**

1210 **4).**

1211 (A) Boxplots show the results of gene regulatory network analysis in each cluster for the top 20

1212 regulons with 10 times runs. NE clusters show high activities of ASCL1 and PAX6, PC cluster

1213 shows high activities of ESRRB and ESRRG, and Ent cluster shows high activities of CDX2 and

1214 CDX1. Fundic gland-specific clusters (PG/Neck1, PC, and chief cells) show a high activity of

1215 SP5.

1216 (B) RNA-ISH of SP5 showing no signal detection in PG and IM. Scale bar: 50 μm.

1217 (C) Expression of APOA1 is limited in the enterocytes.

1218

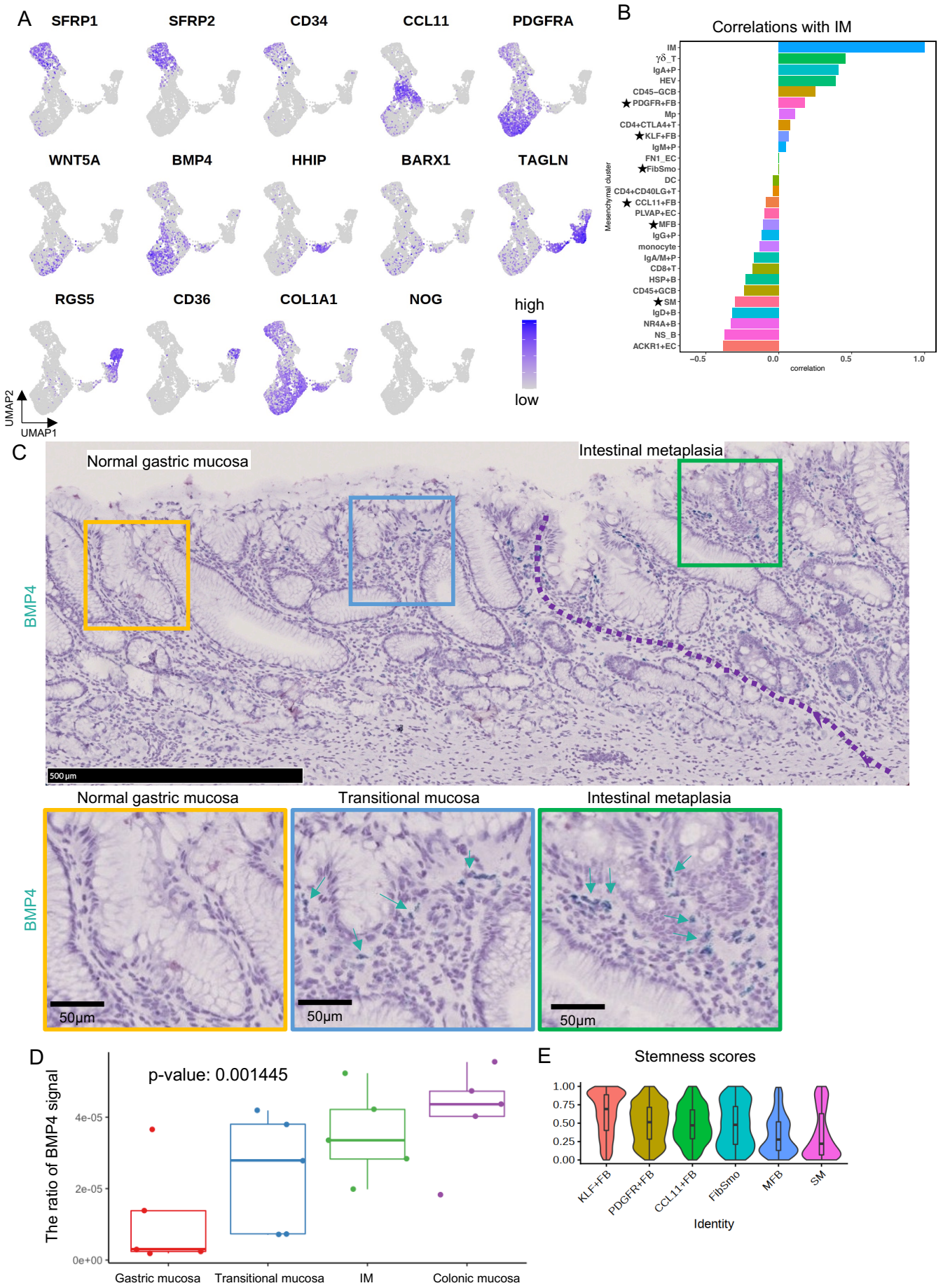
A
SFRP1
SFRP2
CD34
CCL11
PDGFRA
WNT5A
BMP4
HHIP
BARX1
TAGLN
RGS5
CD36
COL1A1
NOG
high
low
UMAP2
UMAP1
B
Correlations with IM
IM
γδ_T
IgA+P
HEV
CD45−GCB
★PDGFR+FB
Mp
CD4+CTLA4+T
★KLF+FB
IgM+P
FN1_EC
★FibSmo
DC
CD4+CD40LG+T
★ CCL11+FB
PLVAP+EC
★MFB
IgG+P
monocyte
IgA/M+P
CD8+T
HSP+B
CD45+GCB
★SM
IgD+B
NR4A+B
NS_B
ACKR1+EC
Mesenchymal cluster
−0.5
0.0
0.5
1.0
correlation
C
Normal gastric mucosa
Intestinal metaplasia
BMP4
500 μm
Normal gastric mucosa
Transitional mucosa
Intestinal metaplasia
BMP4
50μm
50μm
50μm
D
p-value: 0.001445
The ratio of BMP4 signal
4e-05
2e-05
0e+00
Gastric mucosa
Transitional mucosa
IM
Colonic mucosa
E
Stemness scores
1.00
0.75
0.50
0.25
0.00
KLF+FB
PDGFR+FB
CCL11+FB
FibSmo
MFB
SM
Identity

1219

1220

1221 **Figure S4. Characteristics of fibroblast subtypes and BMP4-related analysis (related to Figure 5).**

1222 (A) Representative marker gene expression in fibroblasts. WNT5A and BMP4 expressions are
1223 enriched in PDGFR+FB population, and HHIP expression are in FibSmos.

1224 (B) Bar plot showing the correlation between the number of metaplastic cells (the total of enterocytes
1225 and goblet cells) and ratio of each stromal cell to the number of major clusters to which it
1226 belongs. The ratio of PDGFR+FB is positively correlated with the number of metaplastic cells.
1227 Each stromal cell ratio was calculated as the number of each subcluster divided by total cell
1228 number of the same class. Note: the γδ T cell and PDGFR+FB ratio was calculated as the
1229 number of γδ T cells divided by the total number of T cells and the number of PDGFR+FBs
1230 divided by the total number of fibroblasts, respectively. *: Fibroblasts

1231 (C) Another field of RNA-ISH of BMP4 in IM, transitional mucosa, and gastric mucosa in addition to
1232 Figure 4C. In this field of view, the increase of BMP4 expression was also observed
1233 in the metaplastic gland and normal gastric mucosa adjacent to IM. Top panel: A low
1234 magnification of stomach gland including IM, transitional mucosa, and gastric mucosa. Bottom
1235 panel: A high magnification of each gland. The contour colors correspond with the colors of
1236 squares in the top panel. Arrows: BMP4 signals.

1237 (D) The ratio of BMP4 green signal area in the stromal area in the field of view of the mucosal
1238 surface in each gland. The monotonically increase of BMP4 from normal gastric mucosa to
1239 metaplastic and colonic mucosa was observed (p=0.001445, two-sided Jonckheere-Terpstra
1240 trend test).

1241 (E) Stemness scores in the fibroblasts. KLF+FB shows highest score, whereas MFB and SM show
1242 lowest scores.

1243

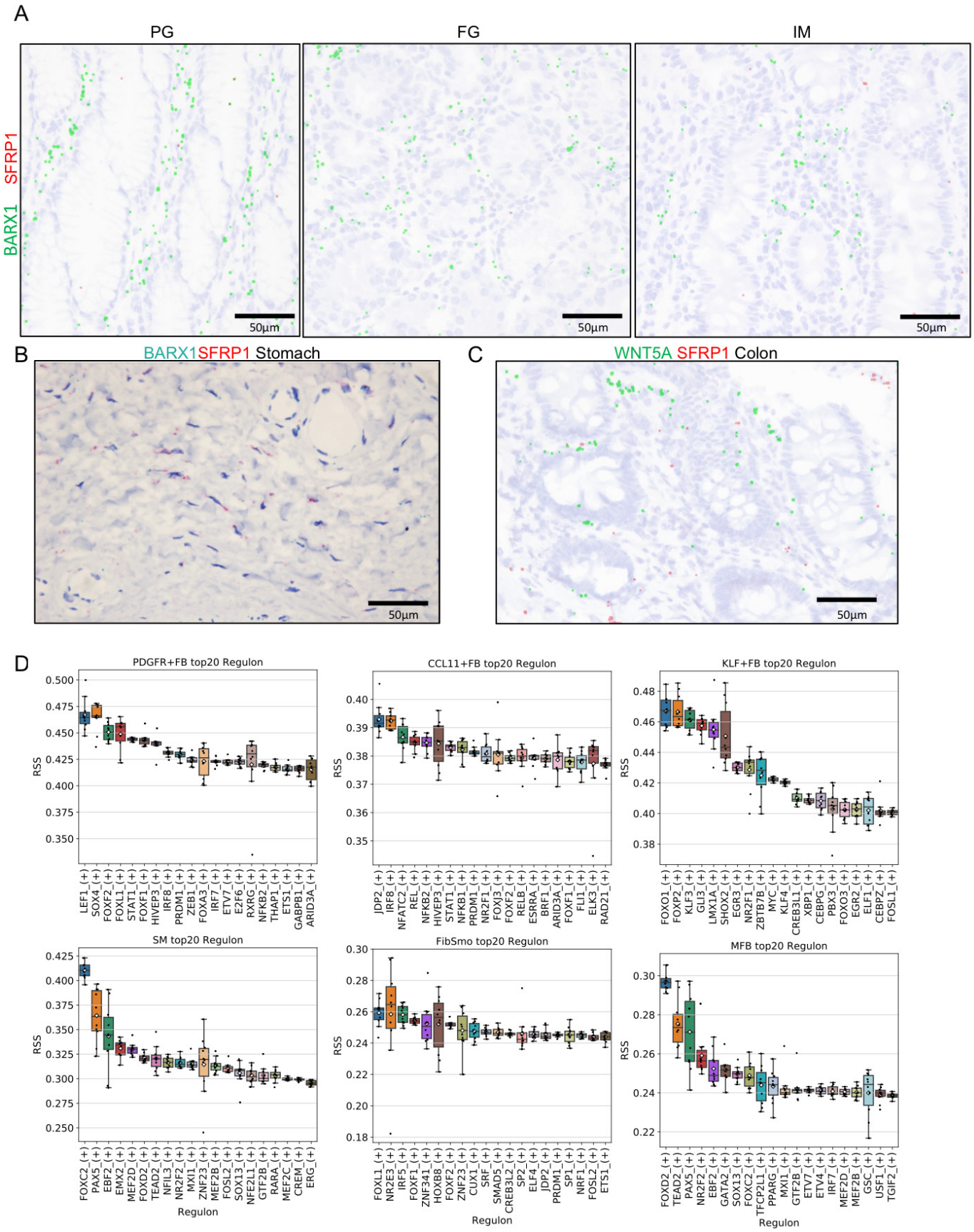
A
PG
FG
IM
BARX1 SFRP1
50µm
B
BARX1SFRP1 Stomach
C
WNT5A SFRP1 Colon
D
PDGFR+FB top20 Regulon
CCL11+FB top20 Regulon
KLF+FB top20 Regulon
SM top20 Regulon
FibSmo top20 Regulon
MFB top20 Regulon
RSS
Regulon

1246 **Figure S5. Spatial distribution of BARX1, SFRP1 and WNT5A in the gastric and colonic mucosa**
1247 **and regulon activity of fibroblasts (related to Figure 6).**

1248 (A) RNA-ISH of SFRP1 (red) and BARX1 (green) showing the lack of SFRP1 and BARX1
1249 coexpression. SFRP1 expression was not observed in the mucosal lamina propria. Each signal
1250 was expanded computationally.

1251 (B) RNA-ISH of BARX1 (green) and SFRP1 (red) in the gastric submucosal region. SFRP1
1252 expression was limited in the submucosa in gastric mucosa. KLF+FBs existed in the submucosal
1253 region because KLF+FBs specifically express SFRP1.

1254 (C) RNA-ISH of WNT5A (green) and SFRP1 (red) in colonic mucosa. SFRP1 was expressed in
1255 mucosal laminar propria in colonic mucosa but not in stomach mucosa.

1256 (D) Boxplots showing the results of gene regulatory network analysis in each cluster for the top 20
1257 regulons with 10 times runs. FOXF1, FOXF2, and FOXL1 transcription activities were
1258 upregulated in PDGFR+ fibroblasts as well as FibSmo cells.

1259

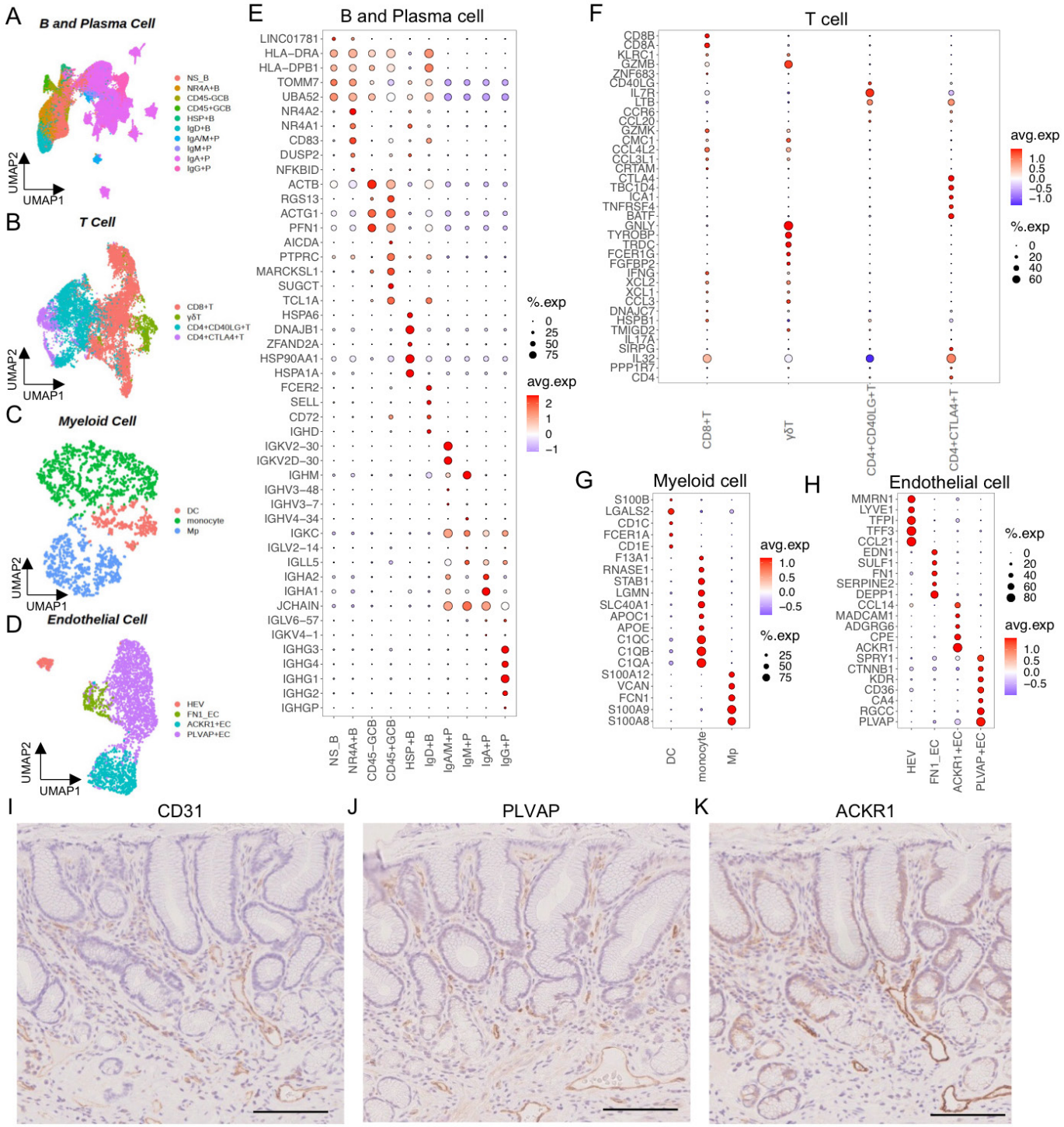

Figure S6. Immune cell and endothelial cell characterization.

(A, E) B and plasma cell UMAP and dot plot showing subcluster marker genes.

(B, F) T cell UMAP and dot plot showing subcluster marker genes.

(C, G) Myeloid cell UMAP and dot plot showing subcluster marker genes.

(D, H) Endothelial cell UMAP and dot plot showing subcluster marker genes.

(I–K) Images of IHC showing the endothelial marker proteins CD31, PLVAP, and ACKR1. PLVAP was distributed in the entire mucosa. Compared with PLVAP, ACKR1 was found in a deeper region. Scale bar: 100 μm.

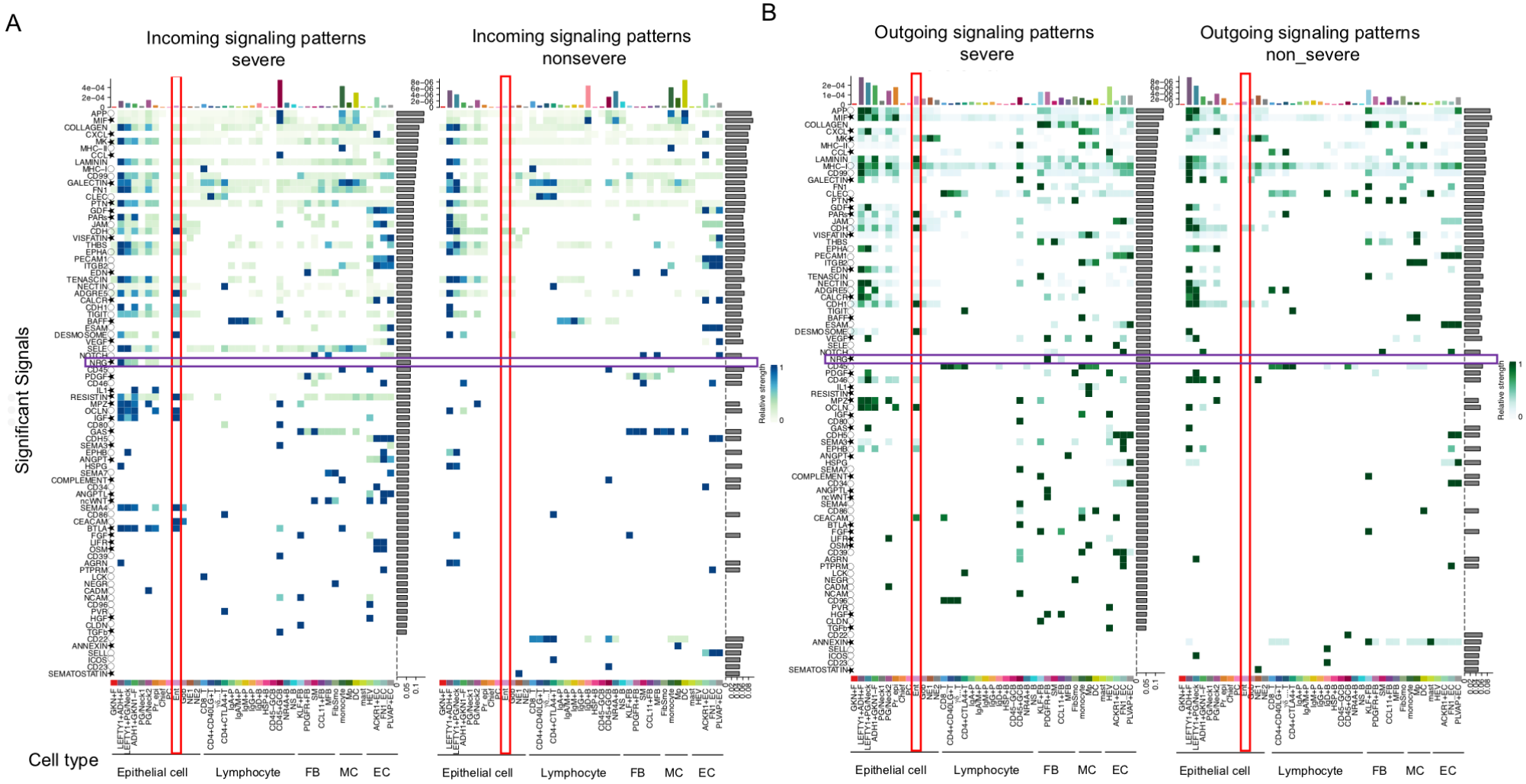
A
Incoming signaling patterns severe
Incoming signaling patterns nonsevere
B
Outgoing signaling patterns severe
Outgoing signaling patterns non_severe
Significant Signals
Cell type
Epithelial cell
Lymphocyte
FB
MC
EC
Relative strength

1270 **Figure S7. Overview of cell–cell communications between IM severe samples and IM**
1271 **mild/moderate samples (related to Figure 7).**
1272 (A, B) Overview of each cell-type and signaling patterns showing more interactions in the enterocytes,
1273 fibroblasts, and myeloid cells of IM severe samples. Top bar plots showing the sum of the
1274 communication probability calculated by cellchat library for each cell type. Right bar plots showing
1275 the proportion of the contribution in each signal to the total. Heatmaps showing relative strength
1276 for each cell type in each signaling. Red square: enterocytes; purple square: NRG signaling; *:
1277 secreting signals; O: cell–cell contact; no symbols: extracellular matrix. Jin et al. (2021) reported
1278 the signal ligand and receptor pair details.
1279

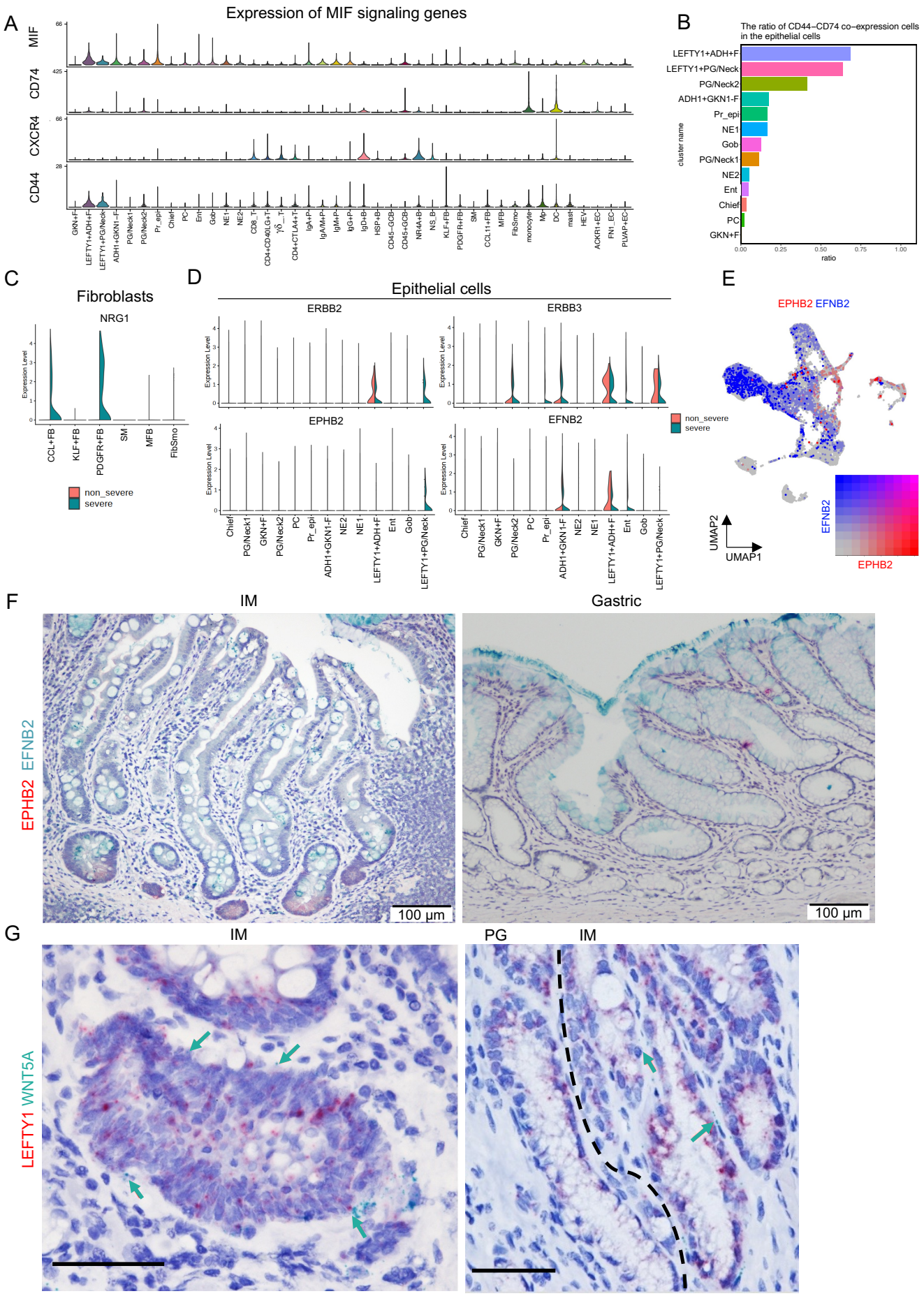
A
Expression of MIF signaling genes
MIF
CD74
CXCR4
CD44
B
The ratio of CD44−CD74 co−expression cells in the epithelial cells
LEFTY1+ADH+F
LEFTY1+PG/Neck
PG/Neck2
ADH1+GKN1-F
Pr_epi
NE1
Gob
PG/Neck1
NE2
Ent
Chief
PC
GKN+F
cluster name
ratio
C
Fibroblasts
NRG1
Expression Level
CCL+FB
KLF+FB
PDGFR+FB
SM
MFB
FibSmo
non_severe
severe
D
Epithelial cells
ERBB2
ERBB3
EPHB2
EFNB2
Chief
PG/Neck1
GKN+F
PG/Neck2
PC
Pr_epi
ADH1+GKN1-F
NE2
NE1
LEFTY1+ADH+F
Ent
Gob
LEFTY1+PG/Neck
E
EPHB2 EFNB2
UMAP2
UMAP1
EFNB2
EPHB2
F
IM
Gastric
EPHB2 EFNB2
100 μm
100 μm
G
IM
PG
IM
LEFTY1 WNT5A

1280

1281 **Figure S8. Representative expression of ligand and receptor genes and proteins in the**
1282 **transcriptional profile and human tissue (related to Figure 7).**

1283 (A) Violin plots showing MIF signaling genes in the all-cluster cells. CD44 and MIF expressions are
1284 highest in LEFTY1+cells, whereas CXCR4 expression is highest in B cell clusters.

1285 (B) Percentage of cells with CD44–CD74 coexpression in epithelial cells. LEFTY1+cells show higher
1286 scores than other epithelial cells.

1287 (C) NRG1 expression is limited in PDGFR+FB and CCL11+FB from IM severe samples. Left half:
1288 expression of cells derived from IM severe samples; right half: expression of cells derived from IM
1289 mild and moderate samples.

1290 (D) NRG receptor (ERBB2 and ERBB3) and EPHB signaling (EPHB2 and EFNB2) genes expression
1291 in epithelial cells. Left half: expression of cells derived from IM severe samples; right half:
1292 expression of cells derived from IM mild and moderate samples.

1293 (E) EFNB2 and EPHB2 expression in epithelial cells (blue: EFNB2; red: EPHB2). EPHB2 expression
1294 was enriched in LEFTY1+ cells, and EFNB2 expression is higher in GKN1+F and enterocytes.

1295 (F) IHC of EFNB2 (green) and EPHB2 (red) in IM and PG. EPHB2 expression was observed in the
1296 base crypt of IM samples, and EFNB2 expression was observed in the superficial mucosa both in
1297 IM and gastric mucosa.

1298 (G) RNA *in situ* hybridization of LEFTY1 (red) and WNT5A (green) in IM and PG. WNT5A expression
1299 was observed in the invaginations of IM, showed in Miyoshi et al., 2012. Black dashed line shows
1300 the border of IM and the PG. Arrows: WNT5A. Scale bar: 50 μm.

1301

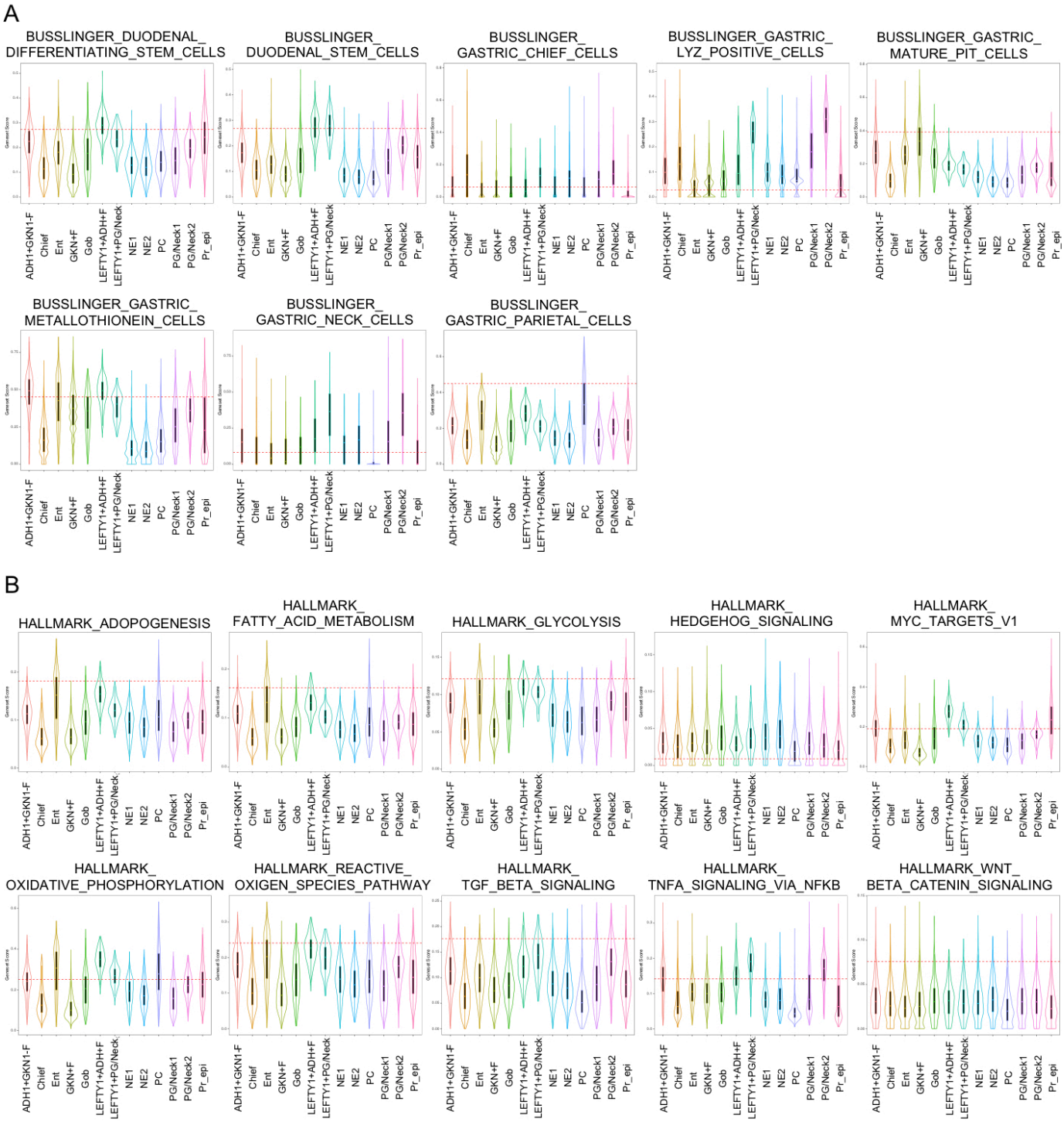

Figure S9. Gene set enrichment analysis of epithelial cells (related to Figures 2–4).

(A) Combined violin plots and box plots showing upper gastrointestinal marker gene scores defined by Busslinger et al. (2021). These gene set scores were clearly enriched in our parietal, chief, and neck cell populations, respectively.

(B) Combined violin plots and box plots showing HALLMARK pathway scores in each epithelial cell. LEFTY1+ cells show high scores of MYC pathway and metabolic-related gene sets such as adipogenesis, fatty acid metabolism, glycolysis, oxidative phosphorylation, and reactive oxygen species pathways.

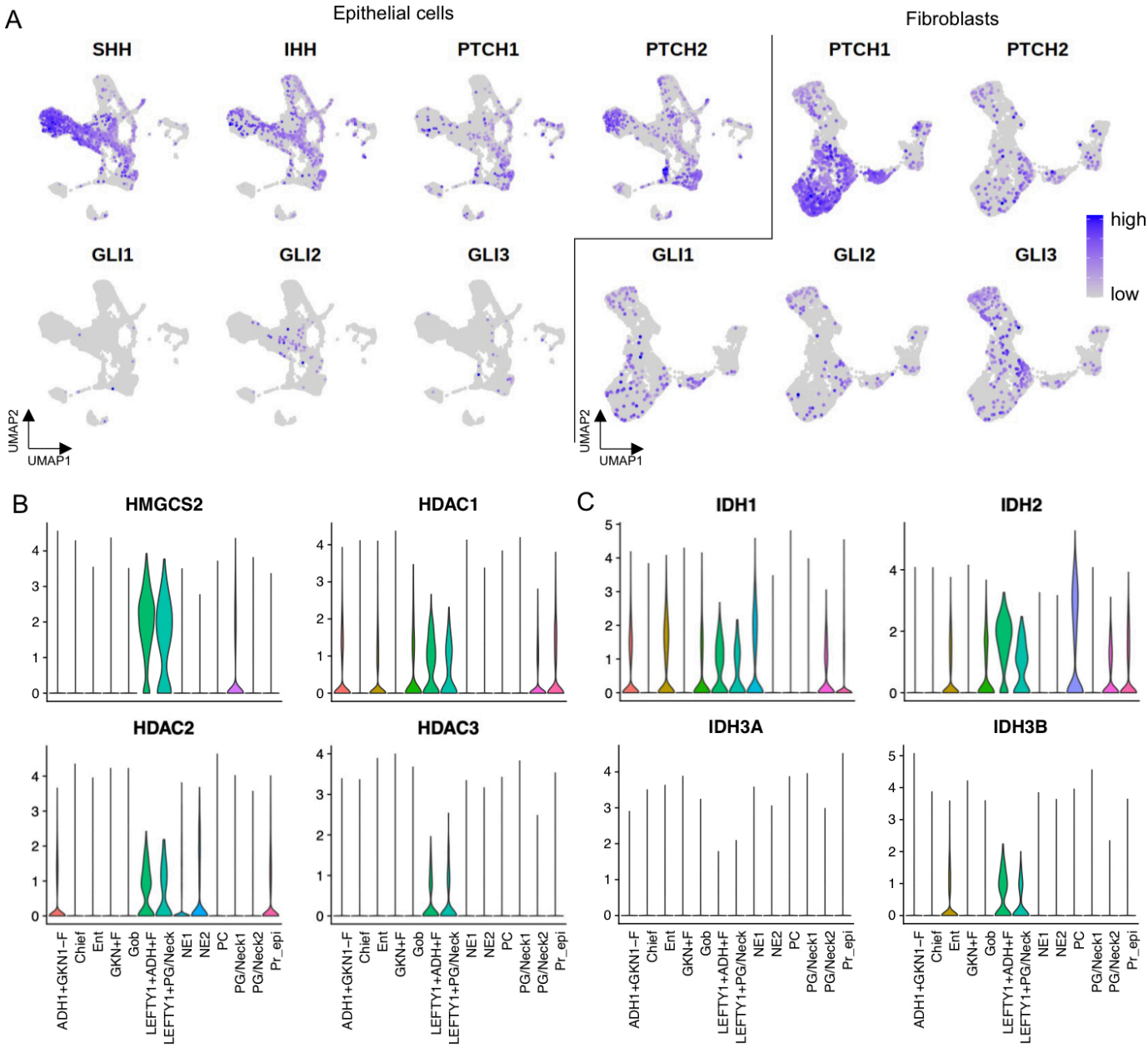

Figure S10. Hedgehog signaling- and metabolite-related gene expression (related to Figure 7).

(A) Feature plots showing hedgehog signaling-related genes. SHH expression is limited in gastric lineage, whereas IHH is expressed in both epithelial cells of gastric lineages and metaplastic lineages, respectively. *PTCH1* and *PTCH2* are expressed occasionally in some PG/Neck1 cells and PDGFR+ fibroblasts, and the downstream effectors of Hedgehog, *GLI1*, *GLI2*, and *GLI3*, are expressed modestly in diverse subtypes of epithelial cells and fibroblasts. Left of the black line: epithelial cells; right of the black line: fibroblasts.

(B, C) Violin plots showing HMGCS2, HDAC, and IDH expression in epithelial cells. Metabolite-related genes are higher in LEFTY1+ cells.